

MECH0020 Individual Project

2019/2020

Student:	Auguste Pugnet
Project Title:	MR safe Master/Slave robotic platform for MRI-guided cardiac catheterization.
Supervisor:	Dr Helge Wurdemann

Word Count: 7399

Declaration

'I, Auguste Pugnet, confirm that the work presented in this report is my own. Where information has been derived from other sources, I confirm that this has been indicated in the report.'

Abstract

The most common cause of death worldwide is cardiovascular diseases (CVDs), some of them such as coronary artery or aorta disease, can only be diagnosed using a procedure called cardiac catheterization. During this process, a long, narrow tube called a catheter is inserted into a blood vessel in the arm or leg and is guided to the patient's heart with the aid of an X-ray machine.

X-ray imagery has been the default tool used to guide the catheter within the patient's body. However, it outputs a 2D image, which is not convenient for a 3D environment that is the body. Over the last decade, magnetic resonance imagery (MRI) has drawn increasing attention to that matter. Indeed, its high contrast 3D image output has proven it to be more suitable to guide the catheter.

An MRI machine is primarily composed of a giant magnet. Thus, metallic components (i.e. motors, screws, wires etc...) must not be present near it, as they would interfere and prevent it from providing a clear image. That constraint has affected and slowed down the development of robots to assist catheterization in that context.

This report introduces a master-slave robotic manipulator which aims at performing precise robot-assisted intra-cardiac catheterization in an MRI environment. Robot-assisted manipulation allows for precise movement and is more suitable to perform a minimally invasive endovascular intervention.

The slave robot is responsible for the translational and rotational movement of the catheter, while relying solely on hydraulic actuators (e.g.: syringes) and MRI-safe materials. The master robot (that is not present in the MRI room) controls the syringes actuation by applying pressure on the fluid using stepper motors. Ultimately, the master and slave robots are connected using plastic hydraulic tubes. The master-slave robot was tested together with a 3D printed heart and a simulated blood flow in order to represent a real-life situation. Results indicate that it could be suitable for medical interventions.

Acknowledgement

I am grateful to my supervisor, Dr. Helge Wurdemann, lecturer in Medical Devices at UCL, for his continuous guidance, advice and support throughout this thesis project. I would also like to thank Shreya Patel for sharing her heart model and providing diagrams to support this thesis.

Table of Contents

DECLARATION	2
ABSTRACT.....	3
ACKNOWLEDGEMENT	4
TERMINOLOGY	8
LIST OF FIGURES.....	9
LIST OF TABLE	14
1.0 INTRODUCTION	15
1.1 PROJECT BACKGROUND	15
1.2 AIM & OBJECTIVES.....	17
2.0 LITERATURE REVIEW	18
2.1 COMMERCIALLY AVAILABLE ROBOTIC PLATFORMS	18
2.2 LIMITATIONS.....	18
2.2.1 <i>Force Feedback</i>	18
2.2.2 <i>Haptic Feedback</i>	19
2.3 CURRENT AND EMERGING MRI DEVICES	19
3.0 A REMOTELY CONTROLLED ROBOTIC PLATFORM.....	22
3.1 OVERVIEW	22
3.2 OPERATING PROCEDURE.....	23
4.0 THE SLAVE ROBOT	25
4.1 ROTATING MOTION MECHANISM.....	25
4.1.1 <i>Rotating Syringe Holder</i>	26
4.1.2 <i>Shaft & Spur Gear</i>	28
4.1.3 <i>Linear Gear Rack</i>	30
4.1.4 <i>Casing</i>	31
4.1.5 <i>Assembly Test Piece</i>	32
4.2 LINEAR MOTION MECHANISM	33
4.2.1 <i>Platform</i>	34
4.2.2 <i>Linear Guided Slot</i>	35
4.2.3 <i>Pushing Mechanism</i>	37
5.0 THE MASTER ROBOT	40
5.1 LINEAR SYRINGE PUMP	40
5.2 ELECTRONIC & CONTROL	42
5.2.1 <i>Hardware Components</i>	42

5.2.3 <i>Code & Programming</i>	44
6.0 EXPERIMENTAL SETUP & RESULTS	46
6.1 ORIGINAL EXPERIMENTAL SETUP	46
6.2 ALTERNATIVE EXPERIMENTAL SETUP	48
6.4 PROTOCOL	50
6.4.1 <i>Experiment 1</i>	50
6.4.2 <i>Experiment 2</i>	51
6.4.3 <i>Experiment 3</i>	53
6.5 MEASUREMENTS.....	55
6.6 RESULTS	57
7.0 DISCUSSION.....	58
7.1 LIMITATIONS AND IMPROVEMENTS.....	58
7.1.2 <i>Batteries</i>	58
7.1.3 <i>Rotational Motion Mechanism</i>	58
7.1.4 <i>Linear Motion Mechanism</i>	58
8.0 CONCLUSION & FUTURE WORK	63
8.1 CONCLUSION.....	63
8.2 FUTURE WORK	63
9.0 REFERENCES	64
10.0 APPENDIX.....	66
10.1 ADDITIONAL RESOURCES	66
10.1.1 <i>Syringe Description</i>	66
10.1.2 <i>Linear Syringe Pump</i>	66
10.1.3 <i>MR Compatibility</i>	67
10.2 EVOLUTION OF THE MASTER/SLAVE COMPONENTS	68
10.2.1 <i>Shaft</i>	68
10.2.2 <i>Linear Rack</i>	69
10.2.3 <i>Casing</i>	69
10.2.4 <i>Syringe Holder Mechanism</i>	70
10.2.5 <i>Compressive Plates</i>	71
10.2.6 <i>Alternative Linear Motion Mechanism</i>	71
10.2.7 <i>Assembly Piece</i>	72
10.2.8 <i>Initial Linear Guided Slot & Frame Design</i>	73
10.2.9 <i>Rib</i>	74
10.3 THE CODE	75
11.0 SHREYA'S DESIGN.....	77
11.1 METHODOLOGY	77

11.2 CONNECTOR PIECE.....	78
---------------------------	----

Terminology

Abbreviation	Meaning
TM	Translational Mechanism
RM	Rotational Mechanism
RMM	Rotating Motion Mechanism
RSH	Rotating Syringe Holder
LGR	Linear Gear Rack
ATP	Assembly Test Piece
LMM	Linear Motion Mechanism
SHM	Syringe Holder Mechanism
LGS	Linear Guided Slot
LB	Linear Bearings
PM	Pushing Mechanism
SP	Syringe Pump
BFH	Barrel Flange Holder
PFH	Plunger Flange Holder
SPM	Syringe Pump Mechanism
DOF	Degree of Freedom
FRCV	Front Right Corner View
FLCV	Front Left Corner View
BRCV	Back Right Corner View
BLCV	Back Left Corner View

Note that all dimensions used are in millimetres.

List of Figures

Figure 1: (a) The slave catheter manipulator of the Magellan system (b) Niobe Vdrive magnetic catheter navigation system (Stereotaxis)	18
Figure 2: The interventionalist applies traditional motion on the input catheter in the sensory system shown on the left and the MRI- compatible manipulator shown on the right replicates that motion on a patient catheter(adapted from(4)).	19
Figure 3: (a) Bending actuation unit that transmits the linear hydraulic actuation of rolling diaphragm into rotary motion. All hydraulic actuation units and the robot body are made of MR Safe materials. (adapted from (2)). (b) Novel robotic platform with versatile, MR-safe slave robot (right) and intuitive master device (left) for endovascular interventions. (adapted from (1))	20
Figure 4: (a) FRCV of the assemble slave robot and (b) 3D model slave robot.	22
Figure 5: (a) Detailed top and rear view of the slave robot. (b) FRCV of the slave robot.	23
Figure 6: Experimental setup where (a) is the top view of the slave robot in the MRI room and (b) represents the SP located in the operating room. The blue lines represent the 10m tubes that connect both rooms.	24
Figure 7: (a) FRCV view of the RMM. (b) FRCV of the LMM.	25
Figure 8: Top-right corner picture of the RMM.	26
Figure 9: Elastic deformation of the RSH.	27
Figure 10: (a) FRCV of the RSH with a detailed rear view of the connector piece. (b) Top view of the RSH with a detailed view of the compressive plates.	27
Figure 11: Detailed front and top view of the syringes and compressive plates	27
Figure 12: FRCV of the cable separator with tubes.	28
Figure 13: (a) FRCV of the shaft with a detailed view of the front face. (b) BRCV of the shaft with a detailed view of the rear face.	28
Figure 14: Horizontal cut of the shaft that exposes the sweep cut.	29
Figure 15: FRCV of the spur gear the spur gear and shaft assembled together.	29
Figure 16: Detailed left view of the LGR.	30
Figure 17: FRCV of the rotating mechanism where (a) is a detailed view of the rear face of the LGR with a side and top picture of the actual syringe plunger flange.	30
Figure 18: (a) Detailed left view of one half of the casing with dimensions. (b) FLCV of one half of the casing with the rod assembled inside where (c)is a detailed view of the stoppers on the surface of the rod. (d) Exploded view of the casing.	31

Figure 19: (a) Left view of the casing with the syringe in a non-lock configuration. (b) Left view of the casing with the syringe in a lock configuration.	32
Figure 20: FLCV of the casing and syringe assembled together.	32
Figure 21 : (a) FRCV of the assembly test piece. (b) FRCV of the assembly key piece. (c) BRCV of the assembly key piece.	33
Figure 22: (a) FRCV of the linear motion mechanism. (b) Front-right corner picture of the linear motion mechanism assembled.	33
Figure 23: (a) FLCV of the platform with the rib like pieces assembled on. (b) Detailed font and left view of the rib-like piece.	34
Figure 24: (a)Detailed left side view of the platform. (b)Detailed rear view of the platform.	35
Figure 25: Detailed right-side view of the test thickness pieces.	35
Figure 26: (a) Detailed front view of the LGS.	35
Figure 27: FRCV of the RMM inserted onto the LGS.	36
Figure 28: FRCV of the LGS with the rods and linear bearings assembled in.	36
Figure 29 : a) Picture of the right side of the LMM with 3 rods and a loading of 1 Kg. b) Picture of the right side of the LMM with 2 rods and a loading of 1 Kg.	37
Figure 30: Detailed left side view of the pusher.	37
Figure 31: FRCV of the pushing mechanism with a detailed view of the grabber.	38
Figure 32: Detailed view of the pin mechanism that holds the pusher to the LGS.	38
Figure 33: (a) Rear view of the platform with the adapted SHM assembled on. b) BRCV of the platform with the adapted SHM assembled on and detail view of the SHM.	39
Figure 34: FRCV of the SPM.	40
Figure 35: FRCV of a SP.	41
Figure 36: (a) Picture of the right side of the syringe pump mechanism assembled. (b) Detailed back picture of the BFH screwed onto the SPM	41
Figure 37: a) Detailed right side view and front view of the BFH piece. b) FRCV of the barrel flange holder piece.	42
Figure 38: (a) FRCV of the PFH piece. (b) FRCV of the PFH piece with the plunger assembled in. (c) : Detailed front and right-side view of the PFH with dimensions. (d) Detailed picture of the PFH assembled on the SPM.	42
Figure 39: CAD design of the electronics hardware used to control the SP.	43
Figure 40: Actual setup of the electronic hardware that control the SP (without power supply).	43
Figure 41: Left side view of the SPM when un-compressed too much.	44
Figure 42: Left side view of the SPM when over compressed too much.	44

Figure 43: (a) Picture of the front switch that prevents an over-compression. (b) Picture of the switch that prevents the syringe to be ‘un-compress’ too much.	44
Figure 44: The side view makes it apparent that the right pulmonary artery and SVC have now been closed off. The blue section below the left pulmonary artery is also connector that has been added to facilitate attachment to the outlet of the mock circulatory system, as fluid would flow in through the IVC and out through the left pulmonary artery.	46
Figure 45: Front view of the 3D heart model. Blood would usually flow from the SVC and IVC into the right atrium, right ventricle and out through the pulmonary trunk.	47
Figure 46: Picture from above of the alternative experimental setup.	49
Figure 47: (a) Catheter tip view from above. (b) Detailed view of one of the catheter insertion part.	49
Figure 48: Continuous shooting from the front right corner of RMM being actuated by the SP.	50
Figure 49: Continuous shooting from above of the RMM being actuated by the SP.	51
Figure 50: Continuous shooting from the front right corner of the LMM being actuated by the SP.	52
Figure 51: Continuous shooting above of the LMM being actuated by the SP.	53
Figure 52: Continuous shooting from above of the RMM and LMM being actuated together by the two SP.	54
Figure 53: FRCV of the alternative RSH assembled on the slave robot.	59
Figure 54: Illustration of the new RSH that prevents the catheter from moving backward with the LMM. The orange arrows represent the actuation of the compressive plates, the green one represents the actuation of the new RSH and the red one represents the actuation of the LMM. The catheter is represented with a blue line.	60
Figure 55: Use of the RSH as an alternative LMM	61
Figure 56: Picture of the shaft with the four tubes for the alternative RSH.	62
Figure 57: Description of the different syringe parts.	66
Figure 58: a) Picture of the syringes used for the syringe pumps. b) Top picture of the syringe pump mechanism	66
Figure 59: CAD models comparing the initial shaft design to the current rod design.	68
Figure 60: PLA 3D print of the initial version of the current shaft design. PLA was not suitable for this component.	68
Figure 61 : From top to bottom, the evolution of the shaft component. The bottom one represents the current one and the middle one represents a former version (without stoppers on its surface).	68
Figure 62: Different version of the LGR component.	69

Figure 63: a) Picture of the current version of the casing. b) Picture of the old version of the casing. c) Picture of the old version of the casing with the former version of the shaft. d) Picture of the current shaft and casing.	69
Figure 64: a) On the left, a FRCV of the different version of the casing. On the right, a FRCV of the former version of the casing. b) Front view of the different version of the casing (current version on the left).	70
Figure 65: a) Picture of the different version of the RSH (current version on the left). b) Picture of the different connector piece used for the RSH (current version on top). c) Picture of the different version of the holes in the RSH (current version on the left).	70
Figure 66: Different version of the compressive plates (current one : Top-left).	71
Figure 67: a) Support syringe slider that is used to support the weight of the syringe used for the rotating mechanism. b) Representation of the support syringe slider with the syringe on it.	71
Figure 68: (a) Right front corner view of the alternate linear motion mechanism with the use of the support syringe slider. (b) Right side view of the linear motion mechanism with the use of the support syringe slider.	72
Figure 69: Detailed front (on the left) and back view of the assembly test piece.	72
Figure 70 : a) Top picture of the assembly test piece and key piece. b) Top picture of the key pieces used to test the first version of the linear guided slot design (see 10.2.8).	73
Figure 71: Front view of the initial version of the linear guided slot and frame (a).	73
Figure 72: Different version of the rib like pieces to hold the acrylic frames together. The former version is shown in b), c) whereas the current version is shown in a).	74
Figure 73: a) Initial version of the rib like pieces. b) current version of the rib like piece.	74
Figure 74: A front view of the 3D model created prior to mesh cleaning using Autodesk Meshmixer. Blood would usually flow from the SVC and IVC into the right atrium, right ventricle and out through the pulmonary trunk.	77
Figure 75: A posterior view of the 3D model created prior to mesh cleaning using Autodesk Meshmixer. The pulmonary trunk divides into the left and right pulmonary arteries.	78
Figure 76: The inferior view of an example connector which could be attached to the IVC to set up the mock circulatory system. The first part of the connector is the large hollow tube with the correct diameter to allow attachment to the pump apparatus on one end and attachment to the IVC on the other end. The secondary part of the connector is the smallest hollow tube on the right, with the correct diameter to allow insertion of the catheter through this smaller tube without fluid leaking out of the mock circulatory system.	79

Figure 77: :The refined 3D model, where the ventricular surface has been smoothed and the IVC remains open, with a cylindrical attachment below it where the extra connector piece would be attached.

80

List of Table

Table 1: Existing commercial platforms for robot-assisted endovascular intervention.....	21
Table 2: Report of the backlash delay between the SP and the LGR for 5 different trials.	55
Table 3: Comparison of the span of motion of the plunger in the SP compare to the span of motion of the LGR for different distance.	55
Table 4: Average speed of the LGR when actuated with the different speed modes.....	56
Table 5: Report of the backlash delay between the SP and the LMM for 5 different trials.....	56
Table 6: Average speed of the LMM when actuated with the different speed modes.....	56

1.0 Introduction

1.1 Project Background

Cardiovascular diseases such as arrhythmia, coronary disease, aorta disease account for one-third of all deaths worldwide (17.9 million/year) (1)(2). Cardiac catheterisation is a successful therapy; indeed, more than one million cardiac catheterisations are performed annually in the US and the incidence of cardiac procedures requiring catheterization-based treatments has been growing significantly globally (3)(4).

These essentially non-invasive and image-guided interventions are performed by manipulating thin and flexible instruments called catheters and guidewires. The inconsistent thin (< 3mm), long (1.5m) flexible catheter is inserted in the patient's leg (i.e. femoral artery) or arm to reach the artery and the heart. Guiding and manipulating the catheter within the patient's body is a challenging task due to the rapidly deforming cardiovascular tissues(2).

Currently, cardiac catheterization is mostly performed under X-ray fluoroscopy. This technique has a high frame rate, a small pixel size and can locate catheters easily. However, it offers low tissue contrast and provides projection images (planar representations). At most, cardiologists can visualize the catheter and a faint outline of the heart structure (5). Fluoroscopy guided catheterisation exposes both patients and staff to ionizing radiation which raises concerns about the long-term health effects. The UK National Radiological Protection Board (NRPB) has estimated an average risk of developing serious cancer after cardiac catheterisation of about 1 in 2500 for adults and up to 1 in 1000 for children aged up to 5 years old (6).

Recently, Magnetic Resonance Imagery (MRI) has been suggested as an alternative open configuration imaging modality to direct and monitor the procedure, providing improved patient access (7). MRI is a unique modality that offers great image contrast for cardiovascular soft tissues. Indeed, MRI allows for visualisation of ablated tissues, necessary for a catheterization, while they are invisible under X-ray fluoroscopy. MRI also has a high flow temperature sensitivity, multiplanar imaging capabilities and most importantly, the ability to output a 3D representation, rendering it ideal for guiding interventional procedures. The ability to visualize the detailed structure of the heart and blood vessels could considerably reduce the time taken to elucidate the patient's problem (6).

However, the use of MRI is limited by the requirement of nonmagnetic instruments, rather long imaging times (i.e. Low frame rates), and difficulties in patient access due to the narrow tube of the magnet. These issues have previously impeded its employment as a supervision technique (7). Nevertheless, recent developments have revealed that MRI image can be obtained at high frames rates (4).

MRI guidance may become the preferred approach for diagnostic cardiac catheterisation in patients with congenital heart disease. Therefore, major advances aiming at minimizing exposure of the interventionalist and personnel, while preserving procedure efficacy, have promoted numerous MRI-compatible robotically guided catheter manipulators or magnetically guided navigation systems (4). They achieve high spatial resolution along with real-time imaging, precise tool and instrumentation positioning, a reduction of the infection risk during surgery as well as a reduction in operation time (1,3,7,8).

This work proposes the design and experimental evaluation of a novel MRI compatible master/slave robotic platform for the manipulation of standard catheters in diverse imaging environments.

1.2 Aim & Objectives

The project aims to design and MRI compatible robot that can steer a catheter in multiple degrees of freedom at a time. The objectives to achieve it are the followings:

- I. Design a slave robot that can steer a catheter translationally and rotationally.
- II. Interface the slave robot with an MRI compatible master actuation system.
- III. Assemble and test the performances of the master/slave robot in a real-life simulation of a cardiac catheterisation.

Moreover, it must follow the general design criteria for MR compatible robots proposed by Chinzei et al. in the early 1990s which can be summed up in the following clinical requirements (9–11):

- The robot must be compatible with clinically used catheter and 3D cardiovascular navigation system. The robot must enable precise actuation with sufficient degrees of freedom to carry out intracardiac catheterization comparable to a manual control of the catheter.
- In terms of safety, the procedure should be quickly revertible to manual and the robot operation must not pose any hazard to the patient nor the MRI scanner.
- The robot should be compact, lightweight and easy to sterilize.

2.0 Literature Review

2.1 Commercially Available Robotic Platforms

Multiple endovascular robotic systems for cardiac catheterization were developed. The main interventional robotic systems on the market include the Sensei and Magellan robotic navigation systems (Hansen Medical) and the Niobe magnetic catheter navigation system (Stereotaxis) (Fig1)(12). They facilitate electro-mechanical manipulation of catheters in up to 6 DOF and have been successfully used in the clinical context. Other commercial platforms include the Amigo (Catheter Robotics), Aeon Phocus (Aeon Scientific), CorPath GRX (Corindus Vascular Robotics), and the R-one (Robocath). A thorough review of these platforms is provided in (13) and summarized in Table 1.

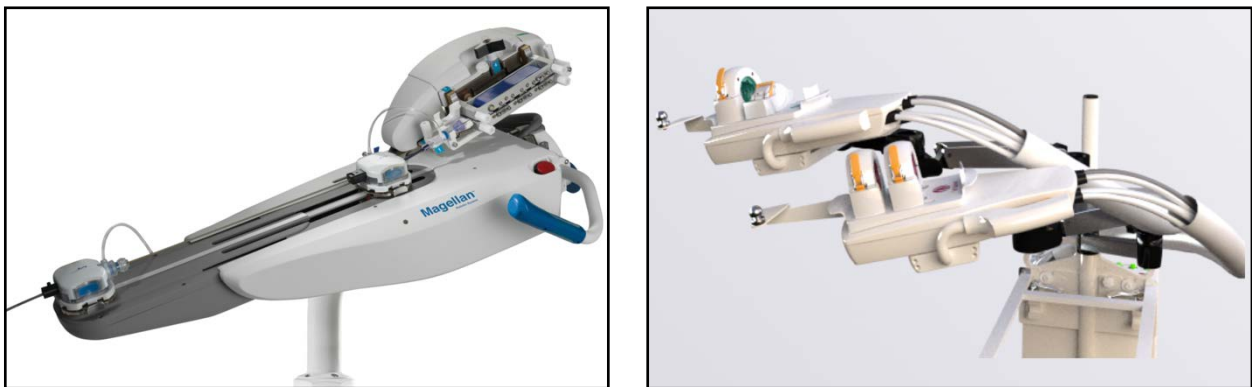


Figure 1: (a) The slave catheter manipulator of the Magellan system (b) Niobe Vdrive magnetic catheter navigation system (Stereotaxis)

2.2 Limitations

2.2.1 Force Feedback

These devices have limitations that affect their employment and popularity in clinical environments including the lack of haptic feedback (except sensei X2) (14). Thus, application of force sensors within the catheters is a growing research area (Table 1). Indeed, in many catheterization procedures, force details from the catheter's tip in contact with the tissue or between the catheter and vessel is advantageous. Excessive catheter force applied onto the vessel walls may cause aggravations such as inflammation, perforation and haemorrhage (12). To avoid these issues, the Sensei robot integrates force feedback based on a proximal force calculation of the catheter with

tactile vibration feedback at the motion controller. A 76% decrease in mean force and a 55% decrease in maximum force were recorded between robotic and manual insertion (12).

2.2.2 Haptic Feedback

Additionally, the control system in most platforms is based on directional buttons or joysticks, thereby undermining the operator's manipulation skills and experience (14). Thus, Tavallaei et al. developed a master robot that observes the interventionalist's traditional motion on an input catheter and replicates that motion through an MR-compatible slave manipulator on a patient catheter (Fig2). Since then, many platforms incorporate ergonomic master manipulators (Table 1).

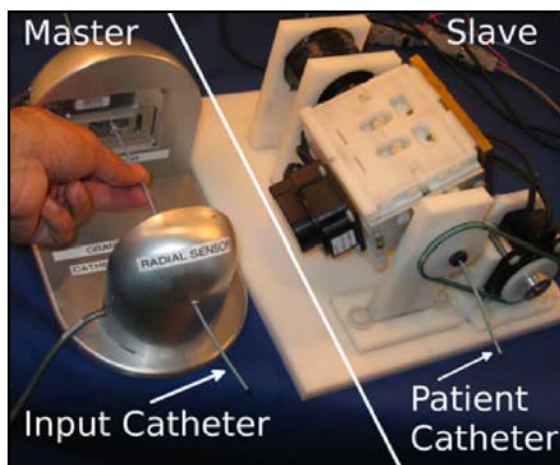


Figure 2: The interventionalist applies traditional motion on the input catheter in the sensory system shown on the left and the MRI-compatible manipulator shown on the right replicates that motion on a patient catheter(adapted from(4)).

2.3 Current and Emerging MRI Devices

Most available robotic platforms now in use are designed to work with X-rays (Table 1). However, future directions tend towards MRI-based interventions (section 1.1). Lee et al. developed an MR safe hydraulic catheter robotic manipulator (Fig3a) (2). Tavallaei et al. also proposed an MRI-compatible system facilitating MRI-guided catheterization (4). They are both able to manipulate commercial MR-conditional steerable catheters and their system was validated in laboratory conditions.

Abdelaziz et al. introduced the CathBot platform which is an MR-safe robot for standard catheter and guidewire manipulation (Fig3b) (1). The slave robot is made of six pneumatic linear stepper motors, three motors for each instrument. All components are made by non-magnetic, non-metallic, and non-conductive materials. Most components are 3D printed, disposable and low-cost.

This project was inspired by the CathBoth platform, it introduces a design and preliminary evaluation of a 3D printable, low-cost MRI compatible novel robotic master-slave platform.

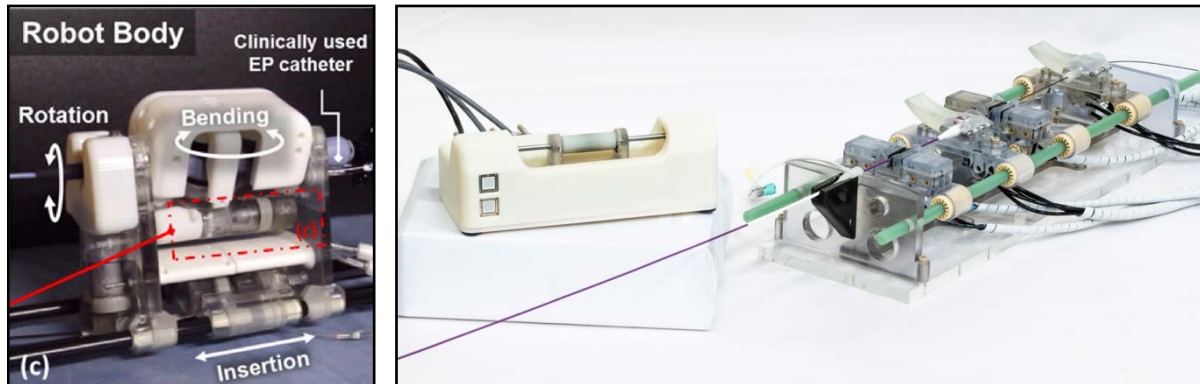


Figure 3: (a) Bending actuation unit that transmits the linear hydraulic actuation of rolling diaphragm into rotary motion. All hydraulic actuation units and the robot body are made of MR Safe materials. (adapted from (2)). (b) Novel robotic platform with versatile, MR-safe slave robot (right) and intuitive master device (left) for endovascular interventions. (adapted from (1))

Table 1: Existing commercial platforms for robot-assisted endovascular intervention.

Platform	Force Sensing	Ergonomic master control system	Suitable for steerable catheters	3D Navigation	MRI compatibility	Date
Sensei® X2 (Auris Medical) (15)	✓	✗	✓	✓	✗	2007
Magellan (Auris Medical) (16)	✗	✗	✓	✗	✗	2015
Amigo (Catheter Precision) (17)	✗	✓	✓	✗	✗	2017
Niobe (Stereotaxis) (18)	✗	✗	✓	✓	✗	2007
Aeon Phocus (Aeon Scientist) (19)	✗	✗	✓	✓	✗	2017
CorPath GRX (Corindus Robotics) (20)	✗	✗	✗	✗	✗	2019
R-one (Robotcath)	✗	✗	✗	✗	✗	2018
Lee et al. (2)	✗	✗	✓	✓	✓	2018
MR-RCNS (Tavallaei et al.) (4)	✗	✓	✓	✗	✓	2013
Abdelaziz et al. (CathBot) (1)	✗	✓	✗	✗	✓	2019

3.0 A remotely controlled robotic platform

3.1 Overview

The design of the MRI compatible robotic platform addresses the clinical requirements mentioned above. A pneumatically actuated robot with two degrees of freedom was developed to manipulate catheters and guidewires by emulating the master control device. The slave robot is composed of two mechanisms, the Linear Motion Mechanism (LMM) and the Rotational Motion Mechanism (RMM). Due to interference with the magnetic field of the MRI scanner, conventional electromagnetic motors cannot be used (3). Various alternative actuation methods were considered such as hydraulics, piezo motors, ultrasonic motors, cable transmission, MR driven ferromagnetic flexible fluidic actuators, air turbines and pneumatic stepper motors (4). Considering budget constraints, plastic syringes accommodated to their appropriate function were selected to operate the slave robot. For the same reason, additive manufacturing (i.e.: 3D printing) was chosen to establish full compliance of the slave robot with the MR safety guidelines (Fig4,5). This approach also facilitates robotic assistance in diverse imaging environments as well as urgent situations in which the robot can be entirely 3D printed and assembled rapidly. Parts like the rubber seals employed in syringes were purchased as the quality is superior compared to 3D printing. The prototype uses transparent commercial plastic syringes as well as transparent laser-cut acrylic sheets, chosen for aesthetic reasons and to favour a better visualisation (Fig4a). However, those components could have been 3D printed instead, without affecting the design performances. Finally, it can be noted that the slave robot is entirely screw-free (Chapter 4.0).

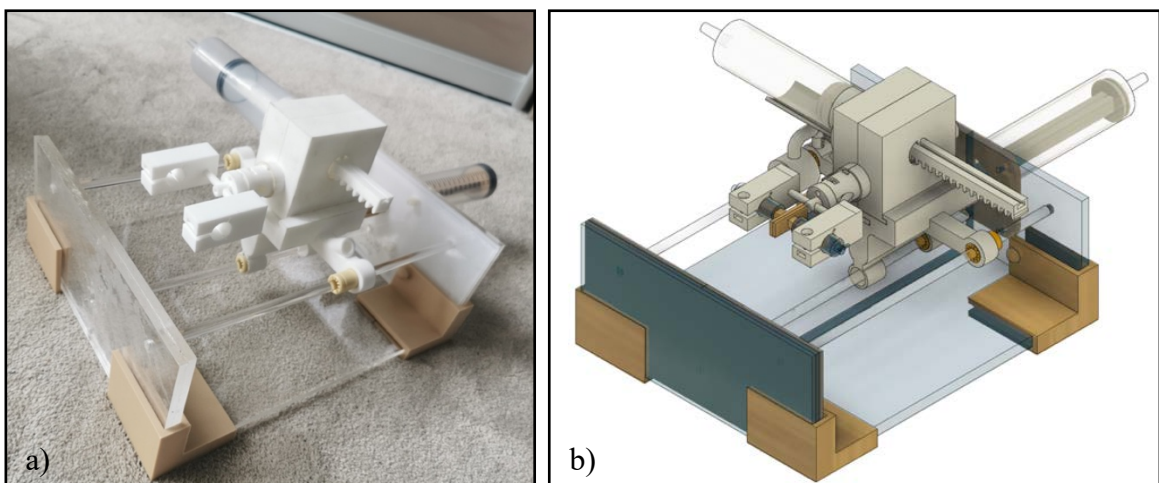


Figure 4: (a) FRCV of the assembled slave robot and (b) 3D model slave robot.

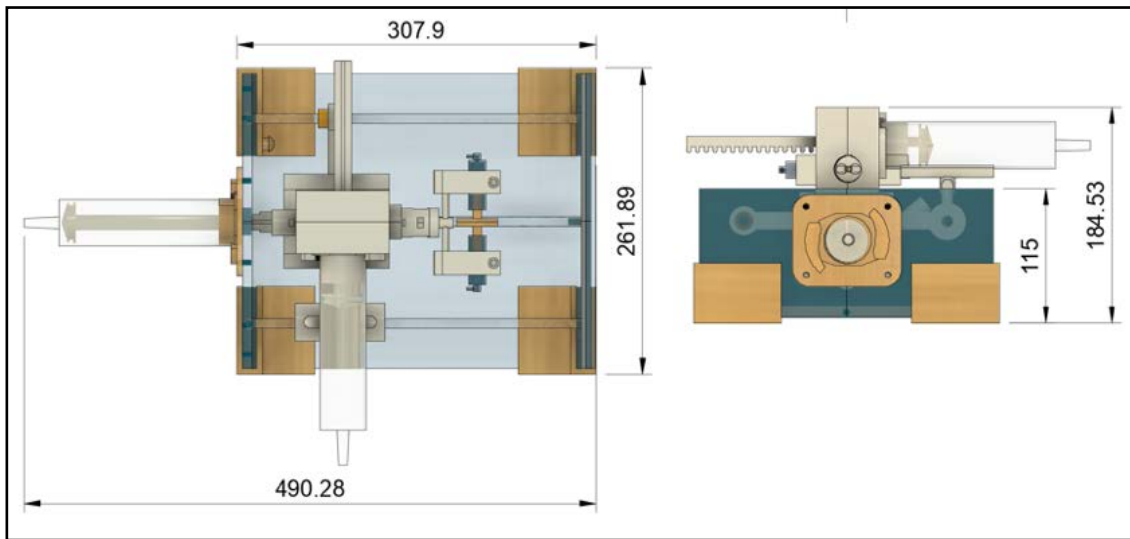


Figure 5: (a) Detailed top and rear view of the slave robot. (b) FRCV of the slave robot.

3.2 Operating Procedure

During an MRI robotically assisted cardiac catheterization, the operator is in the control room which is separated from the operating room (i.e. MR room) by a wall, a door or a window, and has a direct view on the patient (Fig6). The interventionalist commands the master robot using joystick and buttons. The master robot is a syringe pump that utilizes a stepper motor to precisely regulate the span of motion of the plunger that compresses the fluid in the syringe (section 10.1.1). Plastic tubes are used to transfer the work done on the compressed fluid by the syringes in the control room, to the syringes in the MRI room that actuate the slave robot. Contrary to conventional valve based hydraulic systems, hydrostatic transmissions provide a direct fluid coupling between an energy source/sink- most commonly an electric motor and a remote joint (21). Chapter 4.0 lays out the diverse components and features of the Slave robot and Master robot.

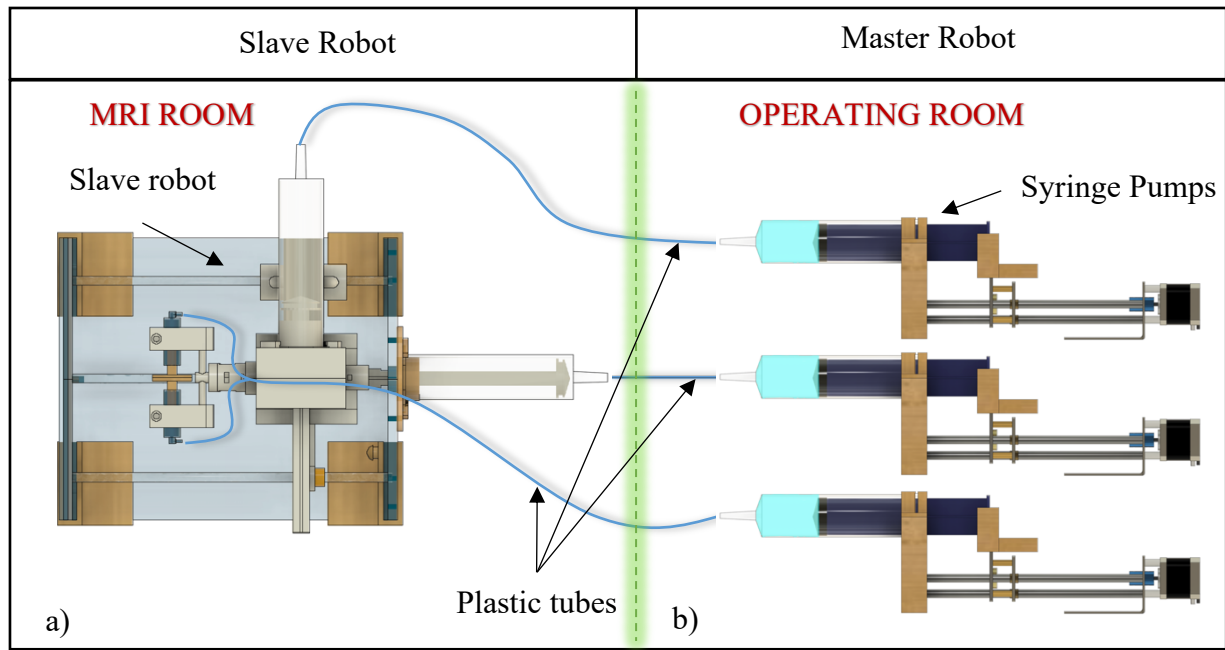


Figure 6: Experimental setup where (a) is the top view of the slave robot in the MRI room and (b) represents the SP located in the operating room. The blue lines represent the 10m tubes that connect both rooms.

4.0 The Slave Robot

The slave robot is the essence of the device; it consists of two fundamental parts that control the two DOF. Although many MRI devices allow for multiple degrees of freedom, few of them manage to actuate their slave robot in more than one DOF at a time.

Pieces were designed to conform together without requiring screws, be reliable, secure and solid enough to perform a catheterization. Nylon and PLA 3D printers were required because some components need to have distinct material properties.

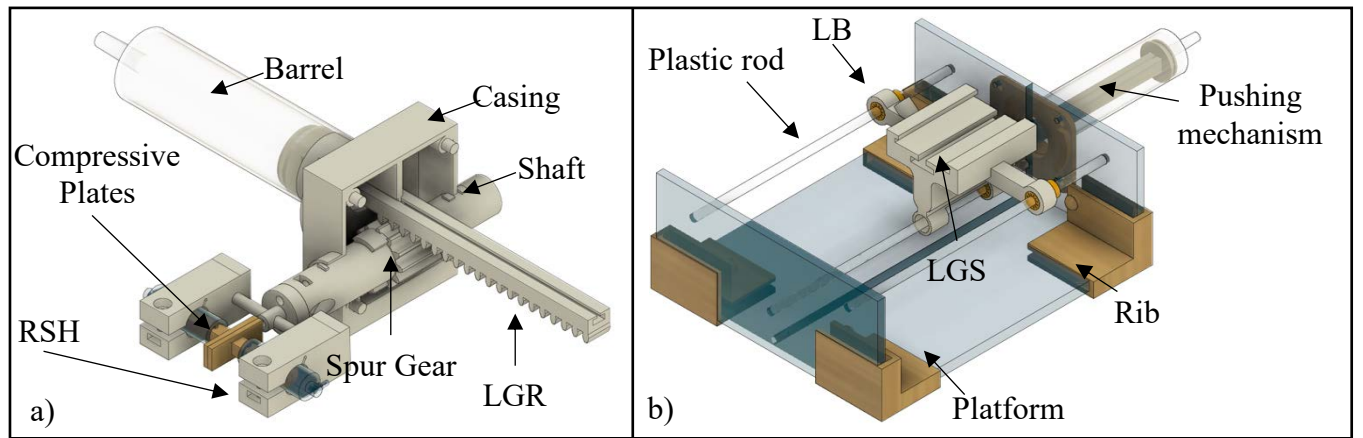


Figure 7: (a) FRCV view of the RMM. (b) FRCV of the LMM.

4.1 Rotating Motion Mechanism

The rotating motion mechanism (RMM) is composed of 7 different pieces (Fig7a). Most parts were conceived using selective laser sintering (SLS). SLS 3D printers utilise filled nylon, which is a mixture of nylon with small particles of a stronger material such as fibreglass or carbon fibre. These mixtures retain the favourable properties of nylon while adding considerable strength and stiffness. Nylon printed parts are remarkably strong and possess high heat/chemical resistance. Most importantly, they acquire excellent resistance to wear, which increases their durability. The quality of print is extremely accurate; thus, the parts have a more refined finish and the professional render pleasantly matches with the medical environment (Fig8).

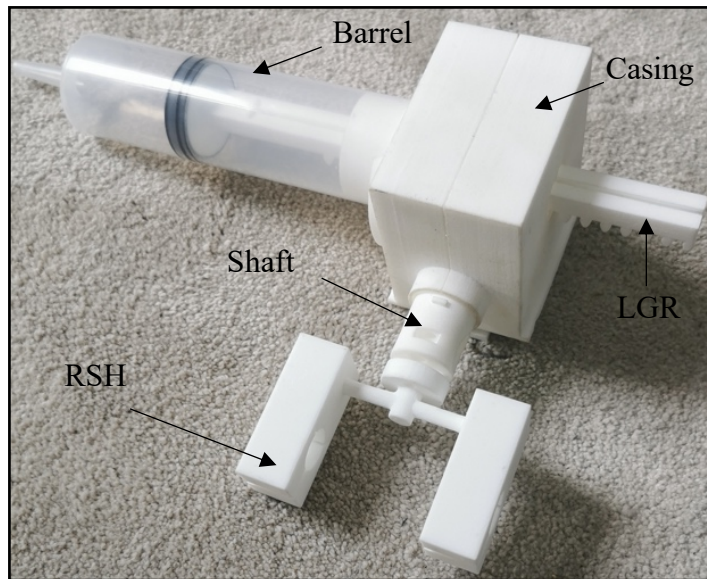


Figure 8: Top-right corner picture of the RMM.

4.1.1 Rotating Syringe Holder

The RSH was fashioned for the catheter to be seized, enabling translational and rotational motions. It can be divided into three parts, the connector piece (A), the arms (B) and the syringe holder (C) (Fig10). The connector piece has one hole in the centre for the catheter and possesses two 3mm holes and two 2mm blind holes on its disk. These holes permit a joint to be made with the shaft that has two pins on one of its edge (Fig13a).

Note: The two 3 mm holes (red dots Fig10a) are not in use in the current version of the RSH. They were made for screws to tighten the RSH to the shaft in case the pin mechanism did not work (red dots Fig13a).

The two syringes must be maintained opposite from one another at any time and the catheter should constantly be at the meeting point (i.e. the centre of the two syringes) of the compressive plates. The holes for the syringes are slightly smaller than the syringes' external diameters (Fig11). Accordingly, to insert the syringe in place, the RSH has to be elastically deformed, inducing a compressive force that secure the syringes in place (Fig9). The holes are 20mm wide to increase the area of contact between the syringes and the tightening mechanism. Finally, to reduce the radial stress that develops on the holes' perimeters when deforming it, two strategically placed grooves were made to prevent a crack from spreading when pressure is applied by the Syringes' barrel.

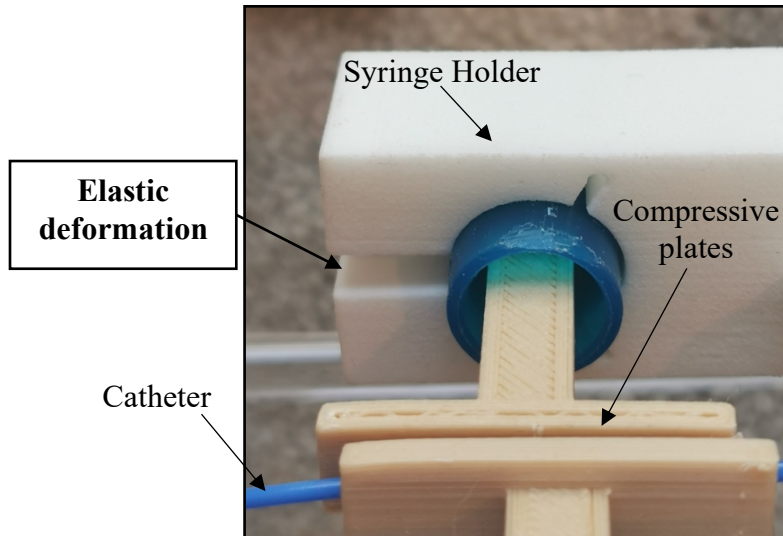


Figure 9: Elastic deformation of the RSH.

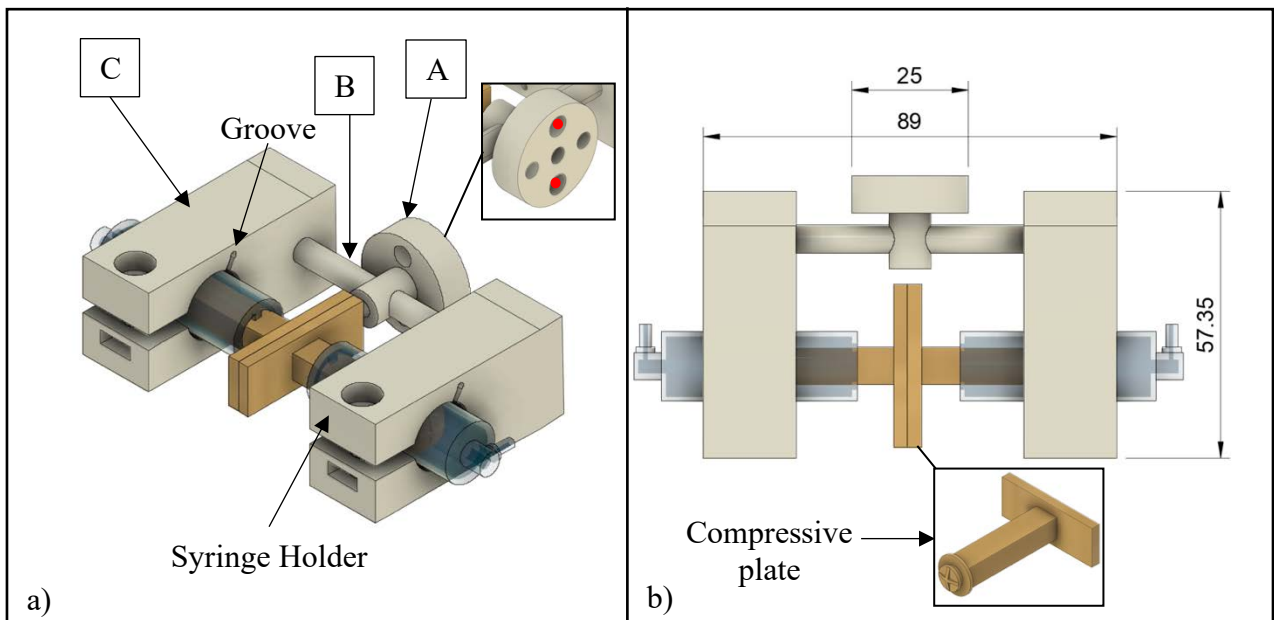


Figure 10: (a) FRCV of the RSH with a detailed rear view of the connector piece. (b) Top view of the RSH with a detailed view of the compressive plates.

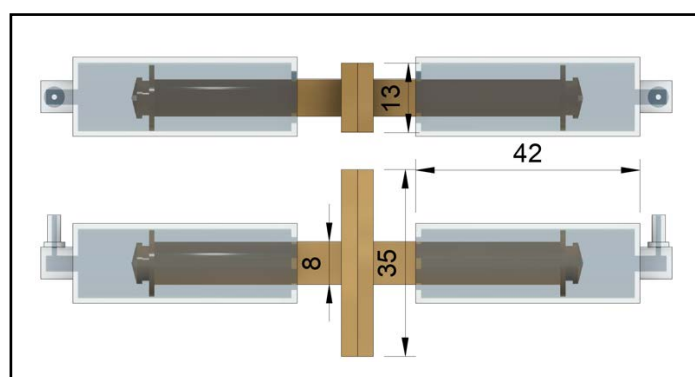


Figure 11: Detailed front and top view of the syringes and compressive plates

4.1.2 Shaft & Spur Gear

The shaft possesses three holes (Fig13). The 2mm catheter (Fig47) is inserted into the middle 5mm hole. When the shaft rotates, the catheter can freely move translationally. The two symmetric holes on the extremities follow a sweeping curve that cuts the inside shaft at an angle (Fig14). The plastic tubes that actuate the seizing syringes (section 4.1.1) must go through those guide holes. Doing so, when the shaft is rotated, those tubes will never get intertwined. Conforming to the shaft and RSH referential, they do not move. The tubes ultimately become entangled as the other end of the plastic tubes is connected to the SP. However, it is preferable that this happens further away from the slave robot to avoid any damages or issues. Cable separators were created to facilitate this task (Fig12).

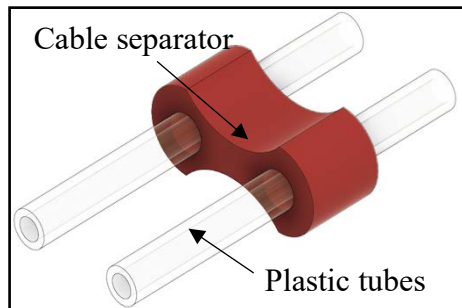


Figure 12: FRCV of the cable separator with tubes.

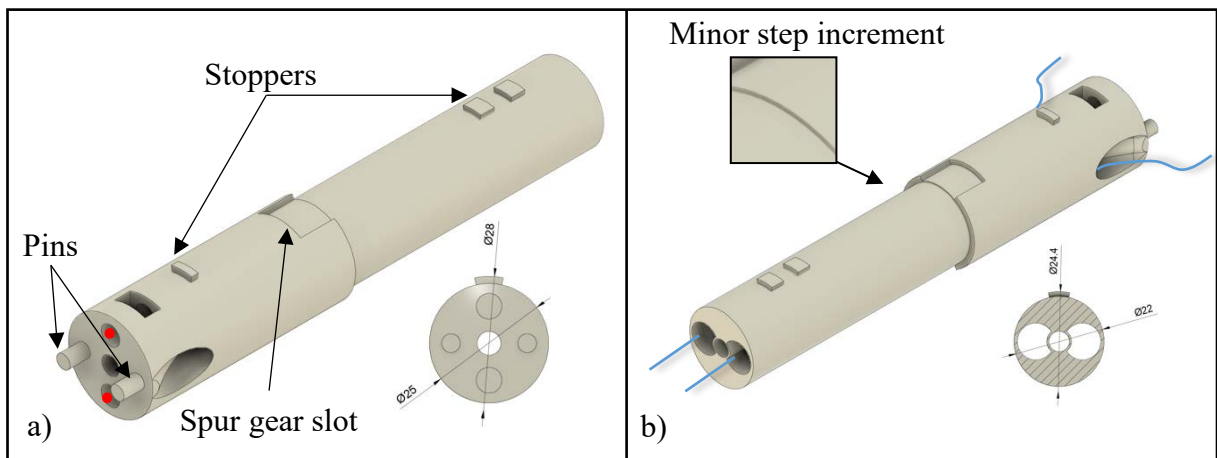


Figure 13: (a) FRCV of the shaft with a detailed view of the front face. (b) BRCV of the shaft with a detailed view of the rear face.

Small extensions on the shaft surface (Fig18b) are used as stoppers to constrain its motion from unwanted movements that could be induced by the LGR (section 4.1.3) or unexpected vibrations, preventing it from moving outside the casing (Fig17). The shaft possesses pins on its edge that connect to the RSH (Fig13). It has a diameter of 25mm on one side and 22mm on the other side to create a slot that greets the spur gear (Fig13b,15).

The spur gear converts the linear motion of the LGR to a rotational motion of the shaft. It was carefully designed to overcome the stoppers on the surface of the shaft (Fig15a) and fit in the slot. Once in place, the spur gear automatically locks itself in. A small increment in radius, akin to a small step on the shaft was built (Fig13b). This small step is slightly bigger than the spur gear's internal diameter. Therefore, the spur gear must be radially deformed to fit in the slot, which produces a compressive force perpendicular to the shaft (normal force) that locks it in place.

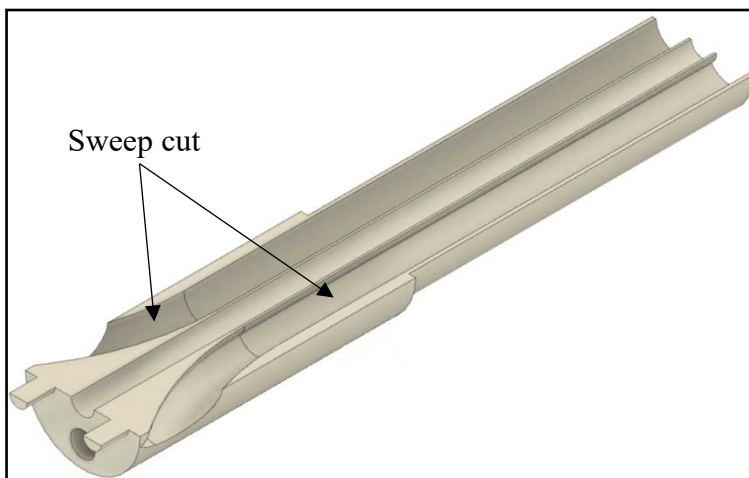


Figure 14: Horizontal cut of the shaft that exposes the sweep cut.

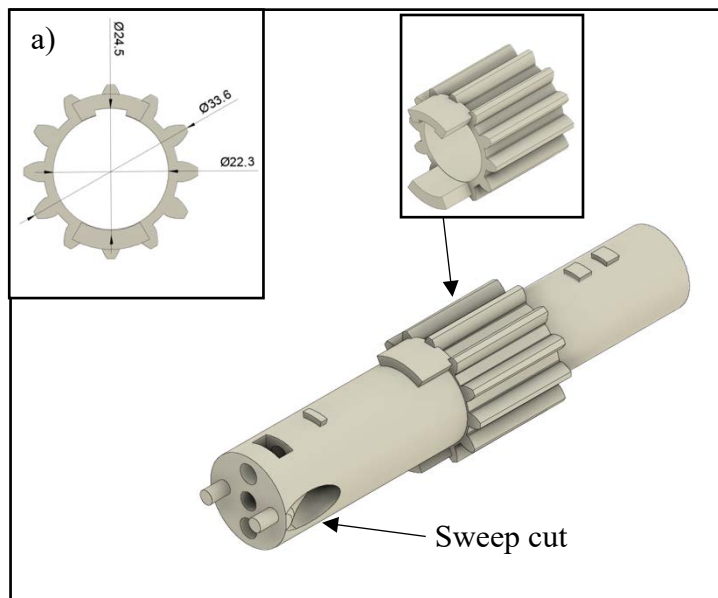


Figure 15: FRCV of the spur gear the spur gear and shaft assembled together.

4.1.3 Linear Gear Rack

The LGR is the motor of the rotating mechanism. It comprises 18 teeth while the spur gear has 12, therefore, when fully extended, the shaft rotates one and a half turn (Fig16). Considering the torsional stiffness of the catheter, some of the energy used to rotate it is lost in elastic deformation. To achieve at least one full rotation, the range of motion was expanded to one and a half turn.

The LGR possesses a T-slot that slides on the casing inverted T-guide to ensure a ‘perfectly’ linear motion that prevents it from moving laterally or twist (Fig17). The end of the LGR was designed to fit in a 150 ml plastic syringe (Fig17a). The plunger was detached from the original syringe, only the rubber seal and the barrel were appropriated. Applying pressure on the fluid actuates the LGR that rotates the shaft, and thus, the RSH.

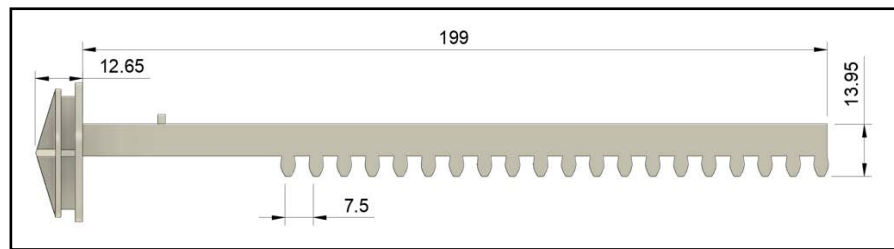


Figure 16: Detailed left view of the LGR.

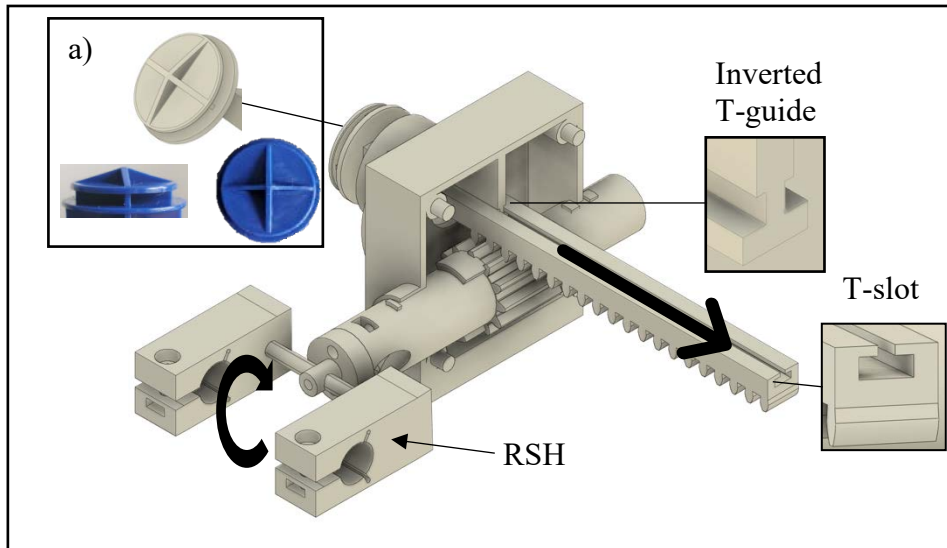


Figure 17: FRCV of the rotating mechanism where (a) is a detailed view of the rear face of the LGR with a side and top picture of the actual syringe plunger flange.

4.1.4 Casing

The casing is the component that encapsulates the rotating motion mechanism. It consists of two pieces that fit together using four pins (Fig18d). The shaft fits in between, where the holes are accustomed to the change in radius of the shaft (Fig18a). The diameters of the holes are 1mm larger than the shaft diameter to provide a free rotation with minimum friction. When the shaft is placed in the casing, the stoppers on the shaft perimeter are on either side of the casing walls, restraining the shaft from sliding outside the casing (Fig18b).

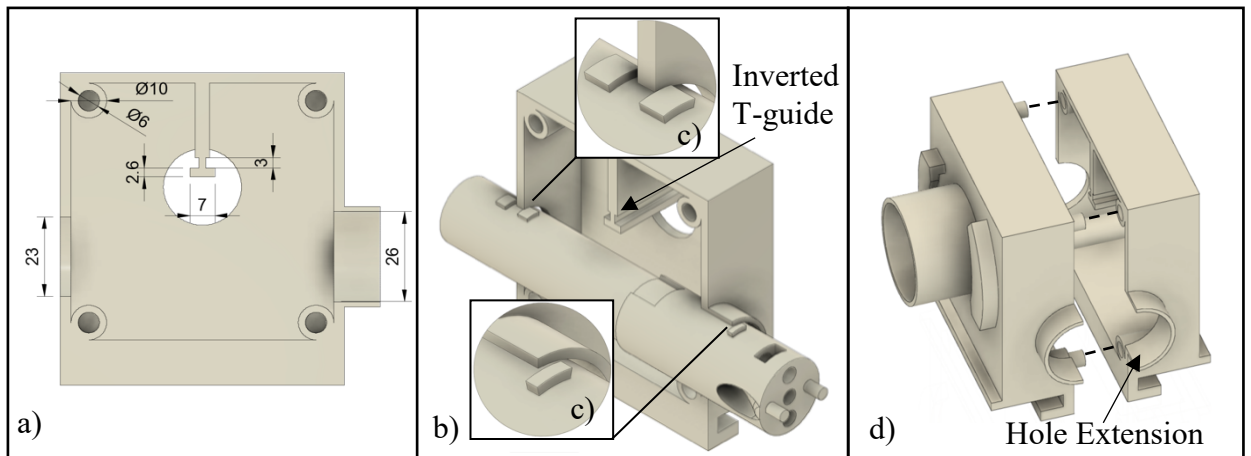


Figure 18: (a) Detailed left view of one half of the casing with dimensions. (b) FLCV of one half of the casing with the rod assembled inside where (c) is a detailed view of the stoppers on the surface of the rod. (d) Exploded view of the casing.

The wall is 5 mm thick to be rigid enough to hold everything and not deform or crack. On the front part of the casing, there is an extension of the hole to guide the shaft, preventing it from moving vertically (Fig18d). On the right side of the casing, there is the SHM, where the LGR is placed in a syringe's barrel and is actuated using pressurized water (Fig20). A simple ‘push and rotate’ lock mechanism, working in two steps has been devised. Firstly, the syringe barrel is inserted onto the hole extension to constrain its motion on the x-y plane (Fig19a). Then, the syringe is rotated 90° clockwise, which locks the barrel flange under the symmetrical locking part and restrains the syringe’s barrel in the z-direction (Fig19b, 20).

Due to the coarse texture of the nylon printed part, when fully locked, the friction force secures the barrel tightly. Finally, the role of the casing is to guide the LGR and ensure it contacts the spur gear. The T-slot of the linear rack slide along the inverted T-guide that extends throughout the casing (Fig17). The guide is aligned with the syringe holder mechanism (Fig18a).

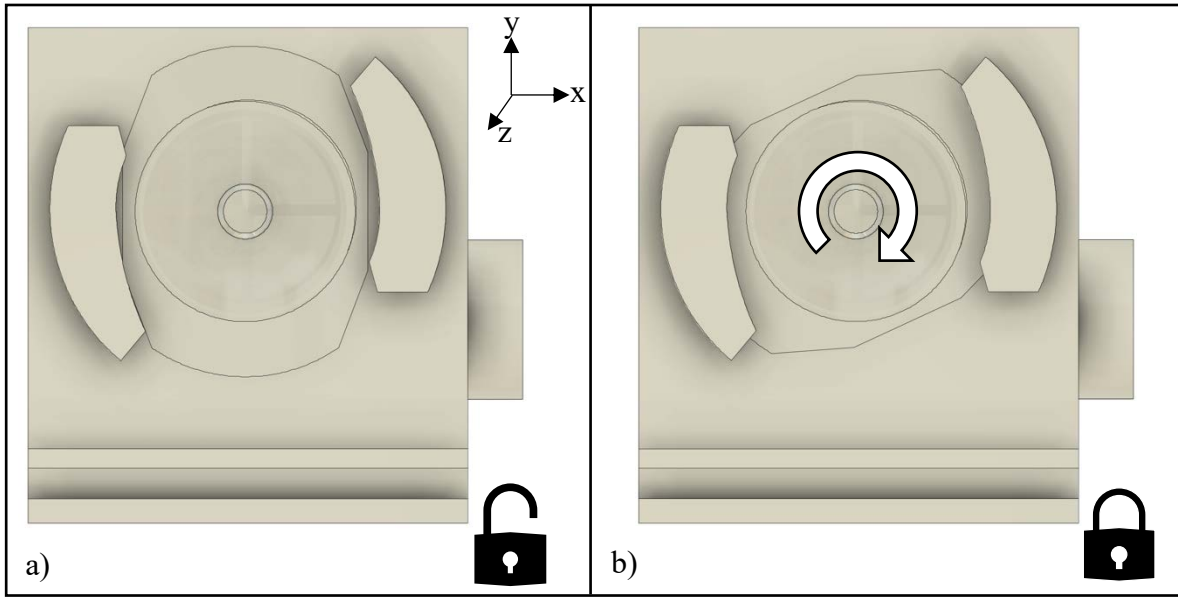


Figure 19: (a) Left view of the casing with the syringe in a non-lock configuration. (b) Left view of the casing with the syringe in a lock configuration.

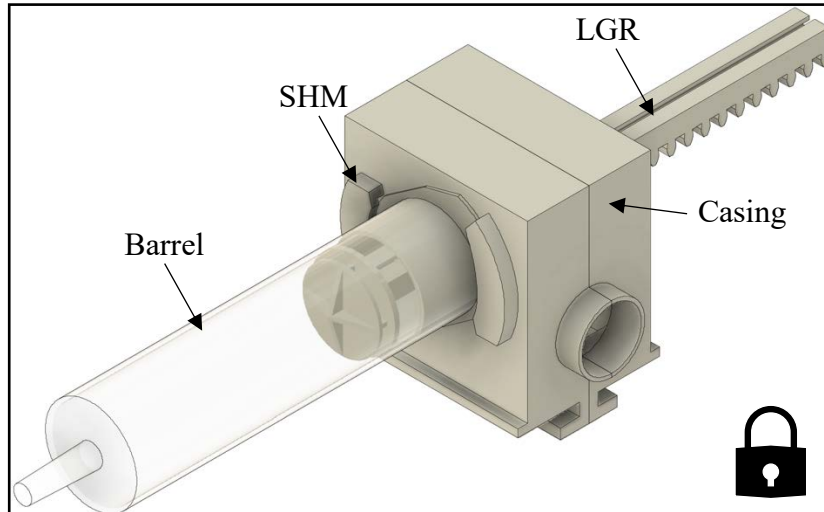


Figure 20: FLCV of the casing and syringe assembled together.

4.1.5 Assembly Test Piece

Most components of the slave robot described above must fit together. Determining the tolerance of a 3D printer is delicate, especially when printing numerous pieces at once with distinctive orientations in the printer. Therefore, if one part does not fit to another because of tolerances error, it can rapidly become a chain's reaction resulting in re-printing or adjusting the CAD model of each component. Printing nylon elements with SLS is also costly and time-consuming. Thus, to reduce the number of print iterations, the assembly test piece (ATP) incorporating all possible holes, pins

and connector, was designed. It is made of two parts, the key and the test piece (Fig21). The key contains a 3 mm hole, a 6 mm pin and a T slot for an initial version of the LGR (section 10.2.8). The test piece consists of 8 different SHM, holes, pins, holes for the linear bearings, slots for the LGR and the first version of the LMM (section 10.2.8). The CAD model of the slave robot was updated with the dimensions of the various connectors according to what was determined with the ATP.

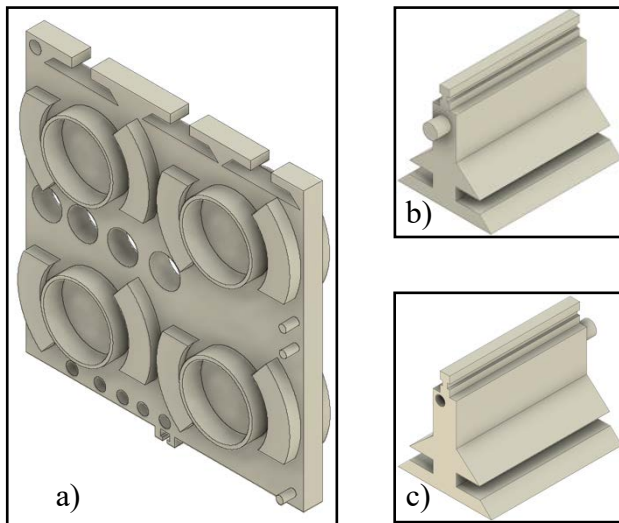


Figure 21 : (a) FRCV of the assembly test piece. (b) FRCV of the assembly key piece. (c) BRCV of the assembly key piece.

4.2 Linear Motion Mechanism

The linear motion mechanism (LMM) permits the catheter to move in a translational direction with a range of motion of 150mm when the syringe is fully extended. It comprises five components, the linear guided slot (A), the linear rods and bearings (B, C), the pushing mechanism (D), the platform (E) and the tightening mechanism (F) (Fig22a).

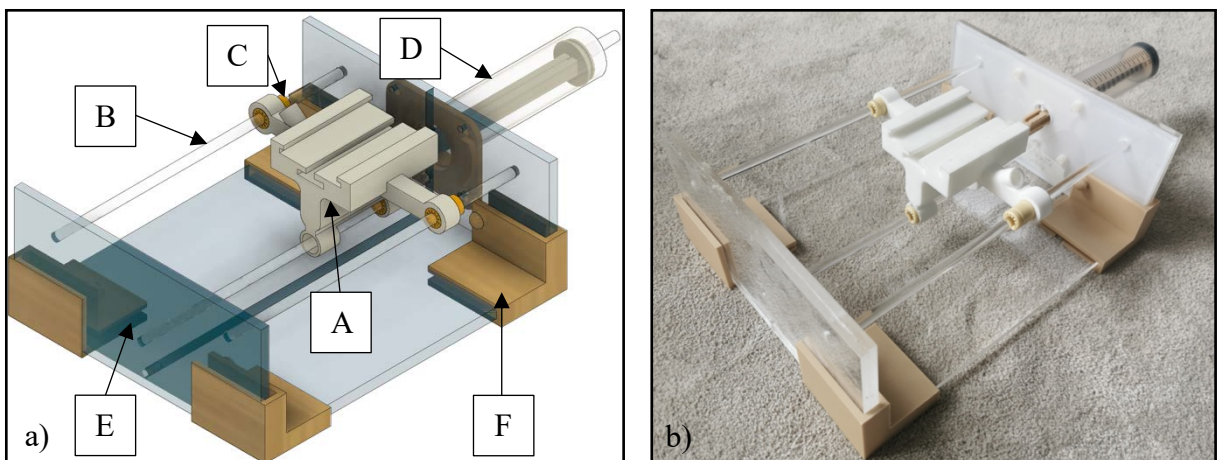


Figure 22: (a) FRCV of the linear motion mechanism. (b) Front-right corner picture of the linear motion mechanism assembled

4.2.1 Platform

The platform is composed of three Perspex frames. The two vertical frames both contain three 8mm blind holes aligned with each linear rod that is inserted into them (A on Fig23). One vertical frame possesses four holes (to attach the SHM), as well as one hole with a T slot guide for the pushing mechanism (B on Fig23,33). Four rib-like parts hold the frames perpendicular to one another (Fig23). They were designed to fit the difference of thickness of the vertical frames (6mm) and horizontal frame (12mm). Following the same approach as with the ATP, different pieces were designed and tested on the platform to determine the thickness that is best suited for the rib-like components, resulting in a thickness of 6.5mm for the horizontal frame and 11.9mm for the vertical ones (Fig23b, 25).

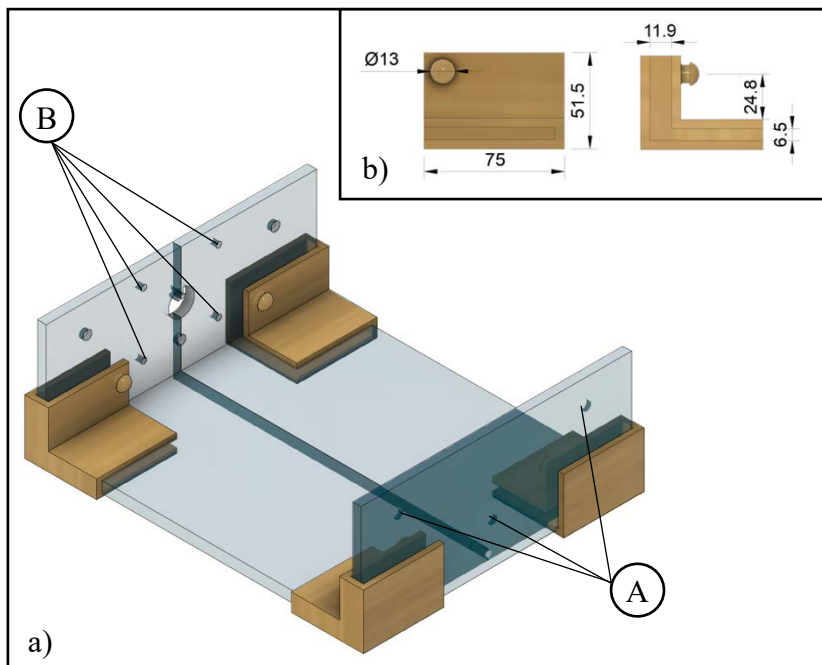


Figure 23: (a) FLCV of the platform with the rib like pieces assembled on. (b) Detailed front and left view of the rib-like piece.

Note: The frames are made of Perspex here, although, in practice, they are planned to be 3D printed in PLA. For that reason, the real platform does not possess the same thickness shown in Fig24a.

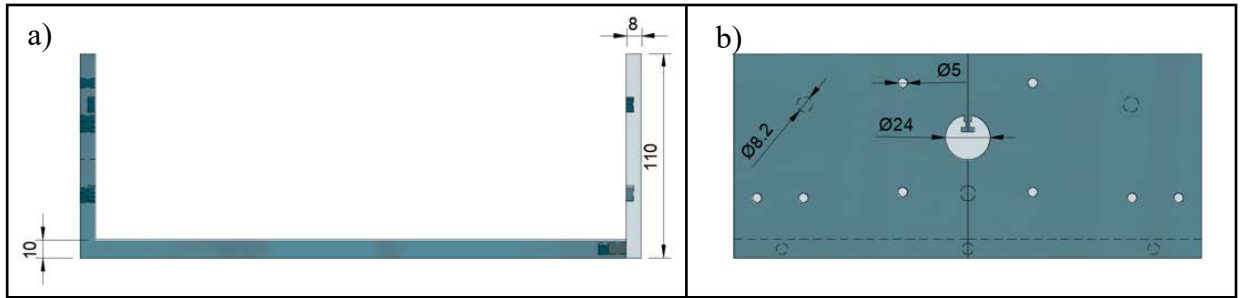


Figure 24: (a) Detailed left side view of the platform. (b) Detailed rear view of the platform.

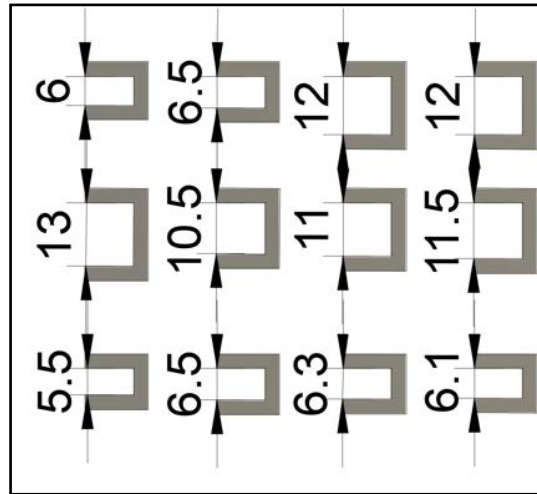


Figure 25: Detailed right-side view of the test thickness pieces.

4.2.2 Linear Guided Slot

The linear guided slot (LGS) is the moving part of the LMM (Fig26). It consists of three arms and a slot on its top into which the casing containing the RMM can be inserted (Fig27). The pieces were created to fit perfectly together while acquiring enough friction to act as a solid joint. The LGS moves with a very small velocity in practice and with negligible acceleration. Thus, there is no potential relative motion of the RMM with respect to the LGS.

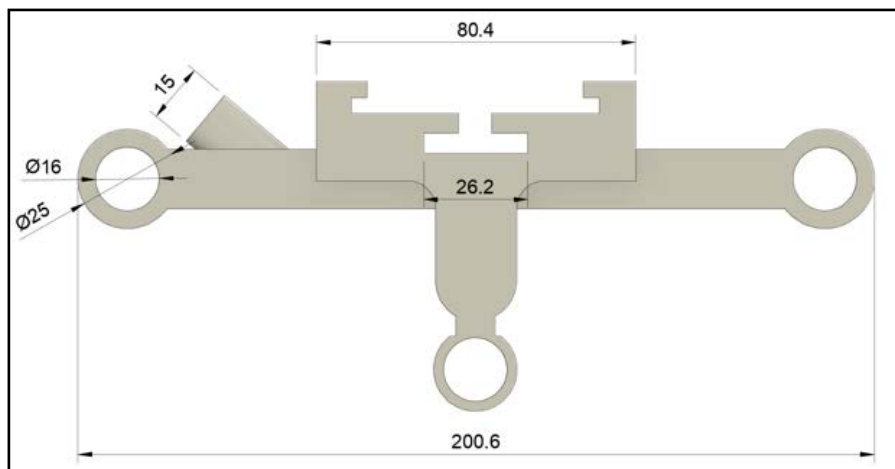


Figure 26: (a) Detailed front view of the LGS.

The LGS is composed of three arms, two symmetric arms on each side and one at the bottom. Each arm contains a 16mm hole on its end where linear bearings (LB) are inserted. The LGS is printed in nylon and hence, has a rough surface that does not easily slide on plastic. Thus, the LB were printed in PLA to ensure smooth motion. LB possess an external diameter slightly bigger than the holes, so they are tightly held in place by radial compressive forces. The LGS can freely slide onto the three 250mm rods that are then inserted into the LB (Fig28).

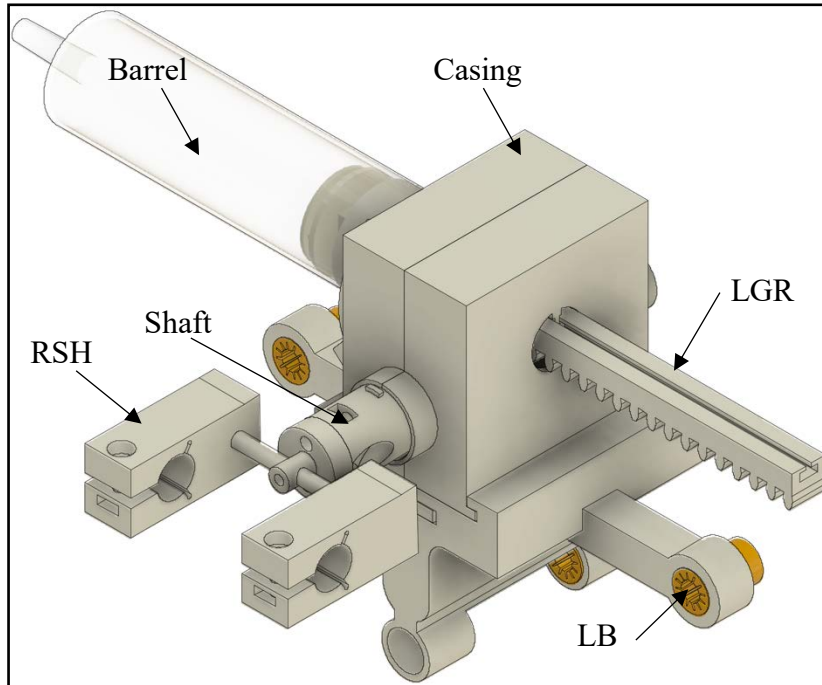


Figure 27: FRCV of the RMM inserted onto the LGS.

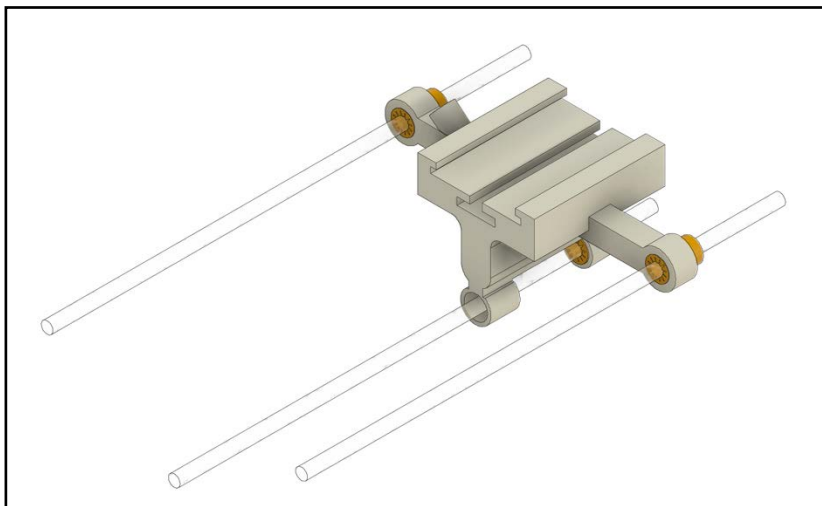


Figure 28: FRCV of the LGS with the rods and linear bearings assembled in.

Two arms and two rods are sufficient to guide the linear motion. However, with two rods, a twisting motion can occur when the LGS is sliding on one side only due to vibration, surface irregularities

or uneven distribution of the pushing force, impacting smooth motion. A third rod highly reduces this effect. Moreover, it prevents the plastic rods from bending, allowing for smoother motion, unaltered by additional friction (Fig29).

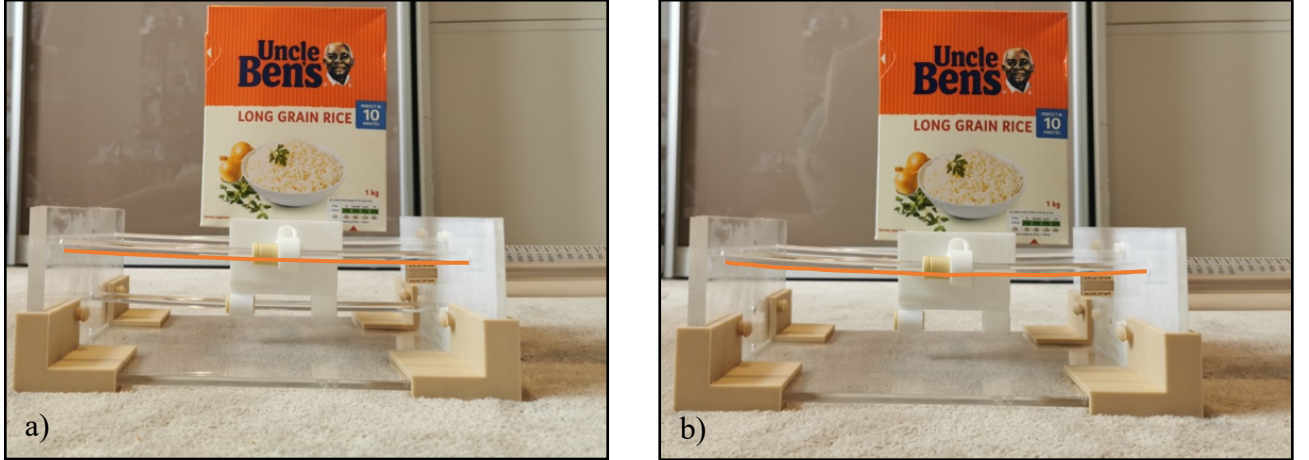


Figure 29 : a) Picture of the right side of the LMM with 3 rods and a loading of 1 Kg. b) Picture of the right side of the LMM with 2 rods and a loading of 1 Kg.

4.2.3 Pushing Mechanism

The pushing mechanism (PM) consists of two parts, the pusher (A) and the grabber (B) (Fig30,31). It was printed in PLA instead of nylon because, as opposed to the LGR, these parts are not susceptible to wear or fatigue. The grabber is fitted at the other end of the pusher and was designed to embrace the shape of the LGS and be held in place adopting a simple pin mechanism (Fig32). The same syringe as the one for the LGR was used, therefore the SHM remains unchanged. The difference is that the SHM was adjusted to be attached to the platform (Fig33).

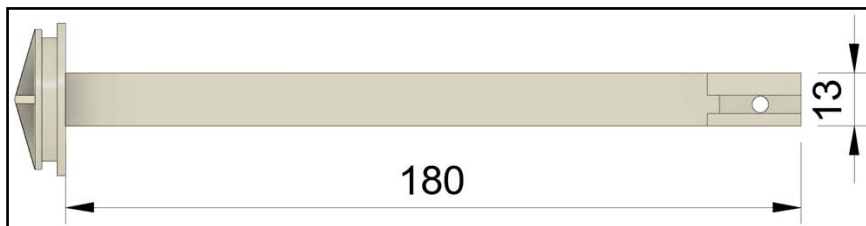


Figure 30: Detailed left side view of the pusher.

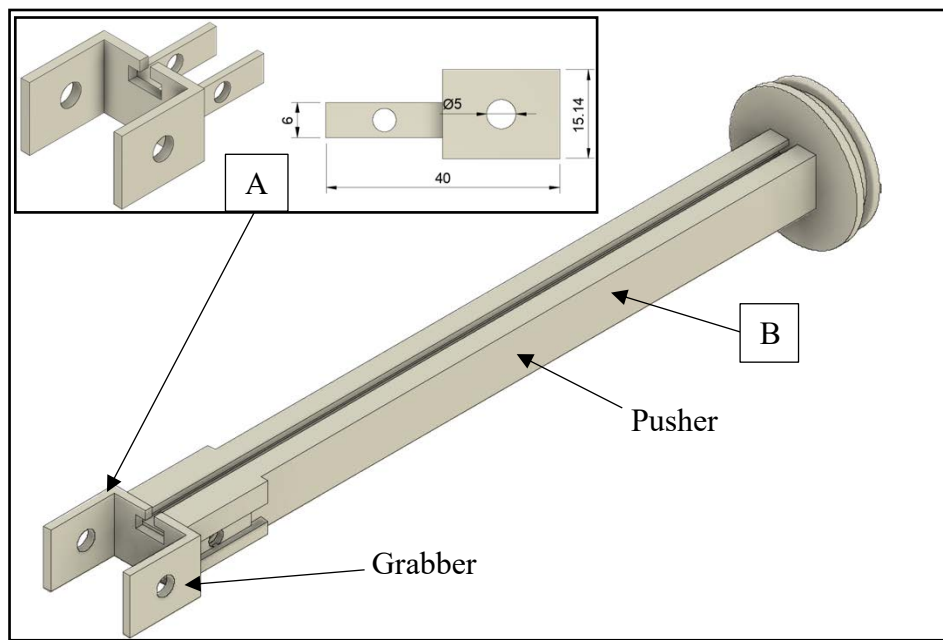


Figure 31: FRCV of the pushing mechanism with a detailed view of the grabber.

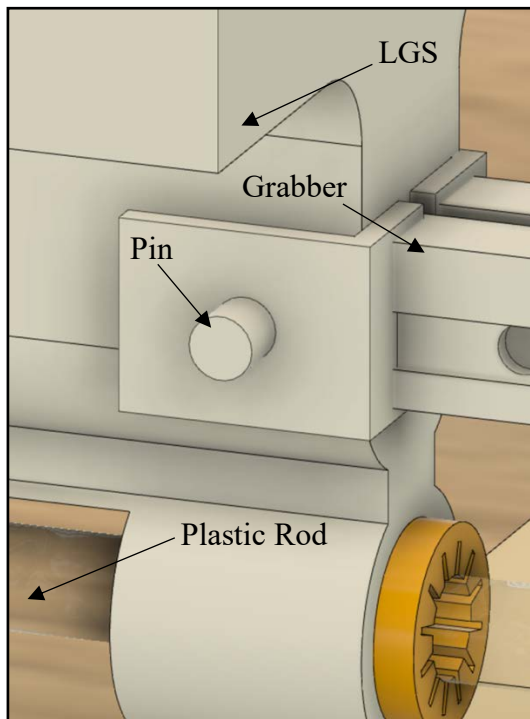


Figure 32: Detailed view of the pin mechanism that holds the pusher to the LGS.

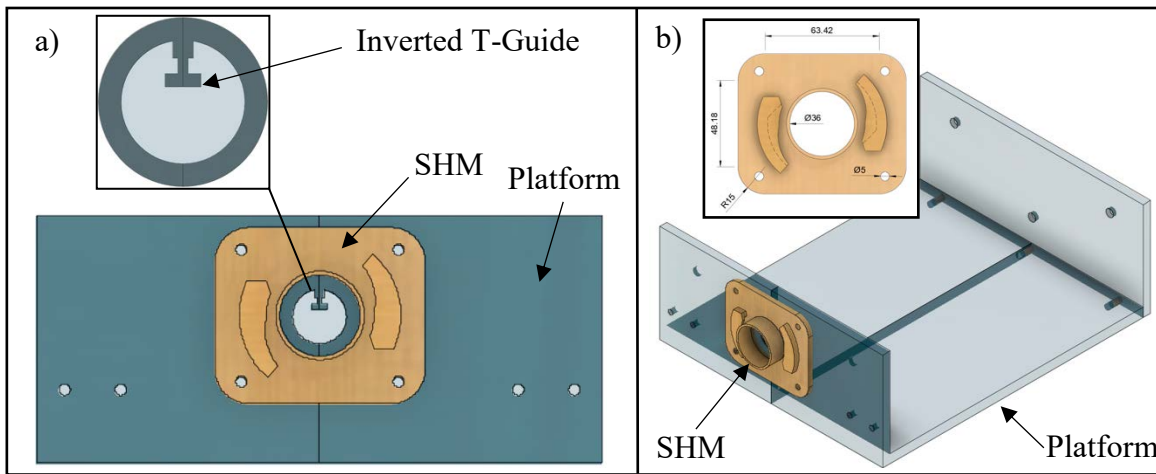


Figure 33: (a) Rear view of the platform with the adapted SHM assembled on. b) BRCV of the platform with the adapted SHM assembled on and detail view of the SHM.

Note: Here, screws are used to attach the SHM to the platform, however, in practice, the platform is not meant to be made of acrylic but entirely 3D printed, so the SHM can be 3D printed on the platform.

5.0 The Master Robot

The master robot is essentially an arrangement of three syringe pumps (SP) that actuate the RMM, LMM and the compressive plates. The SP are controlled by an Arduino board, joysticks and buttons that regulate the stepper motors within the SP. Sterilized water is employed as the working fluid to be clinically safe. The features of the SP are detailed below in addition to the electronic setup.

5.1 Linear Syringe Pump

The motion of the RMM and LMM in the slave robot must be regulated with high accuracy to allow small increment of motion. For that matter, a stepper motor was selected over a DC motor to actuate the SP. In a stepper motor a full revolution is divided into small step increments that are preferable for accurate displacement. The maximum resolution of the stepper motor is 0.15 degree per step. A full rotation can be divided into 2400 steps allowing for a meticulous control of the syringes.

SP are small positive-displacement pumps operated to gradually transfer specific volumes of fluid. They convert the rotating motion of the stepper motor to a linear motion. They have a single lead screw threaded through a pusher block. The pusher block travels when the lead screw turns. The two guide rods keep the pusher block horizontal and perpendicular to the lead screw (Fig34).

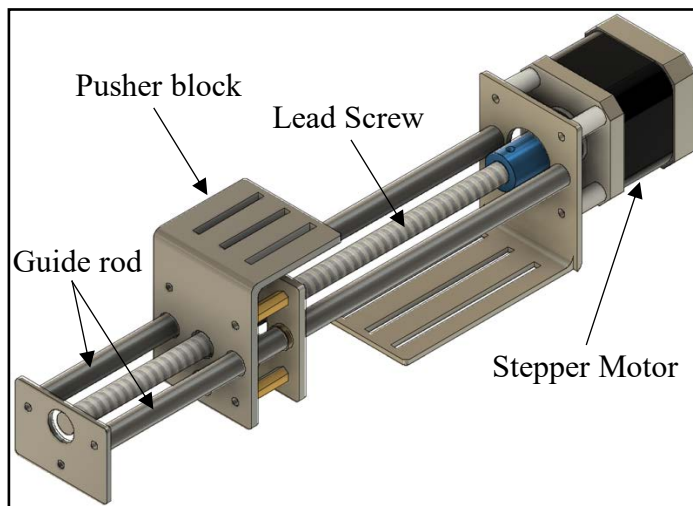


Figure 34: FRCV of the SPM.

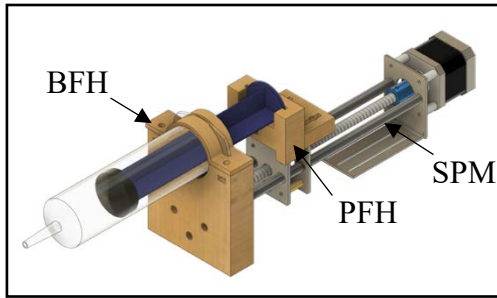


Figure 35: FRCV of a SP.

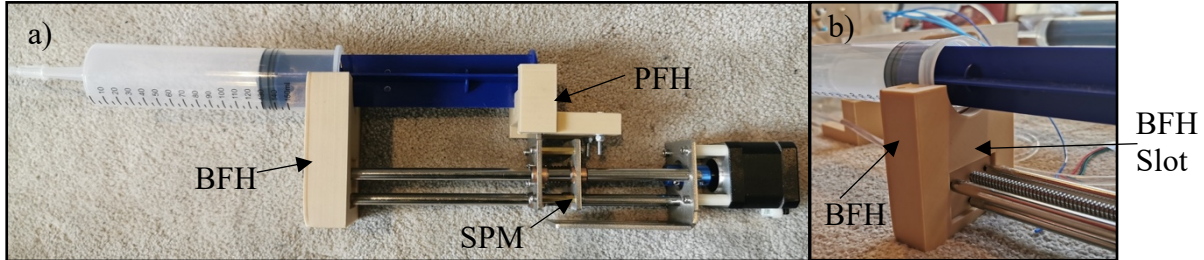


Figure 36: (a) Picture of the right side of the syringe pump mechanism assembled. (b) Detailed back picture of the BFH screwed onto the SPM

The linear motion must be adapted to compress or uncompress the syringe. The SPM was modelled in 3D, then two components were designed to fit a syringe: the barrel flange holder (BFH) and the plunger flange holder (PFH).

The BFH (Fig37) has a slot embedded and screwed at the end of the LMM to constrain the syringe barrel and the barrel flange so that the syringe cannot move at all (Fig35, 36b). The PFH moves with the pusher block (Fig36a, 38d). The plunger flange is completely inserted into the slot (Fig38b).

Note: Those two pieces can be adapted to any syringe on that specific SPM with the dimensions of the plunger flange, barrel, barrel flange and plunger provided. Thus, the range of motion of the LMM and RMM can be adjusted if necessary.

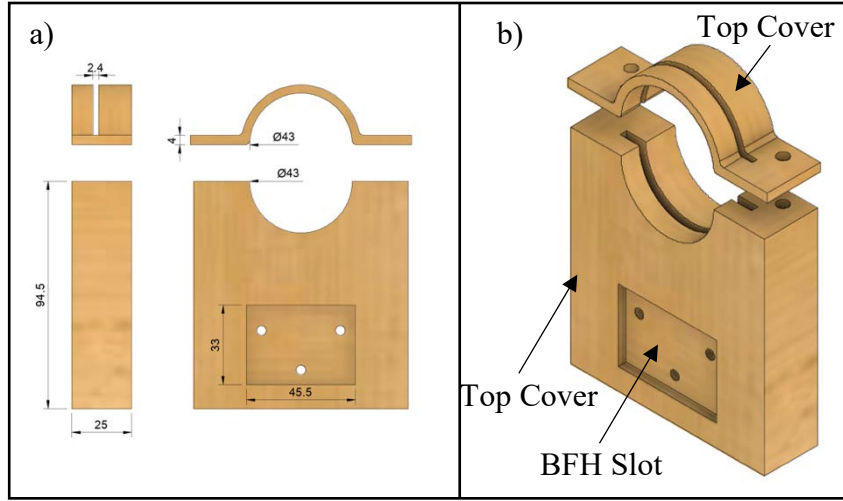


Figure 37: a) Detailed right side view and front view of the BFH piece. b) FRCV of the barrel flange holder piece.

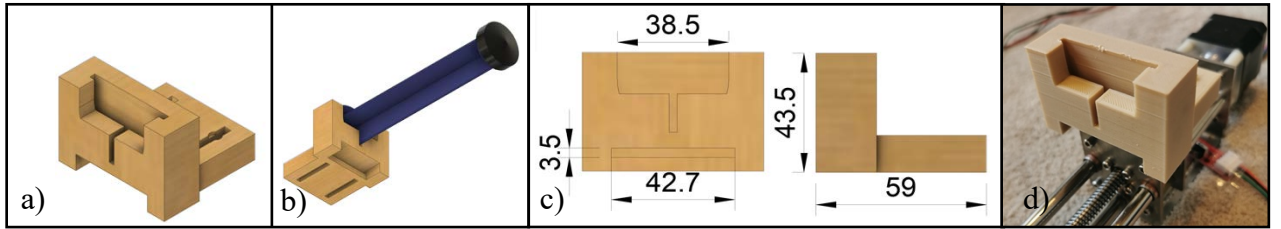


Figure 38: (a) FRCV of the PFH piece. (b) FRCV of the PFH piece with the plunger assembled in. (c) : Detailed front and right-side view of the PFH with dimensions. (d) Detailed picture of the PFH assembled on the SPM.

5.2 Electronic & Control

An affordable control system was designed to accurately regulate the SP and consequently the slave robot. It must allow to fully explore the performance of the master/slave robot. Finally, it must be straightforward and intuitive to handle but also easy to set up and repair.

5.2.1 Hardware Components

The components required for the electronic setup of one SP are an Arduino board, a joystick, two limit switches, an easy driver, a breadboard and a 9V battery supply. The setup is shown on Fig39, 40. The SPM is controlled via a joystick, when the joystick is inclined forward, the stepper motor rotates in one direction and when it is leaned backwards, the motor reverses.

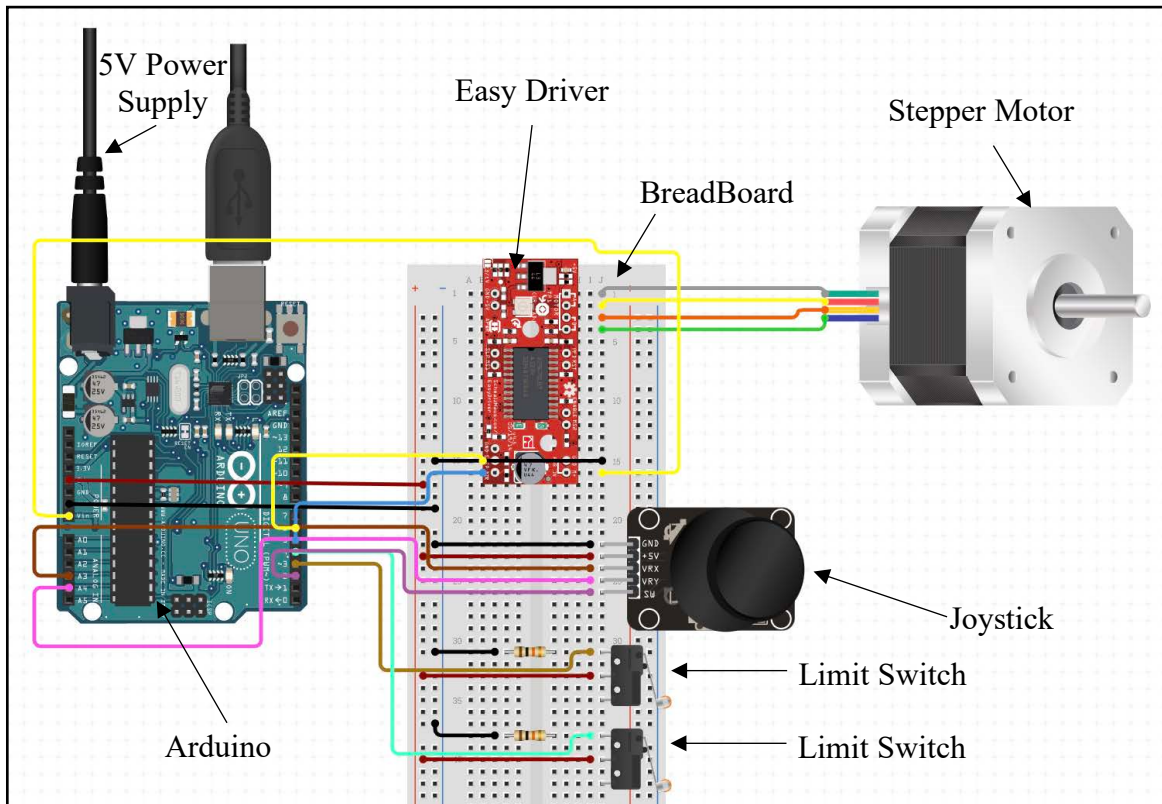


Figure 39: CAD design of the electronics hardware used to control the SP.

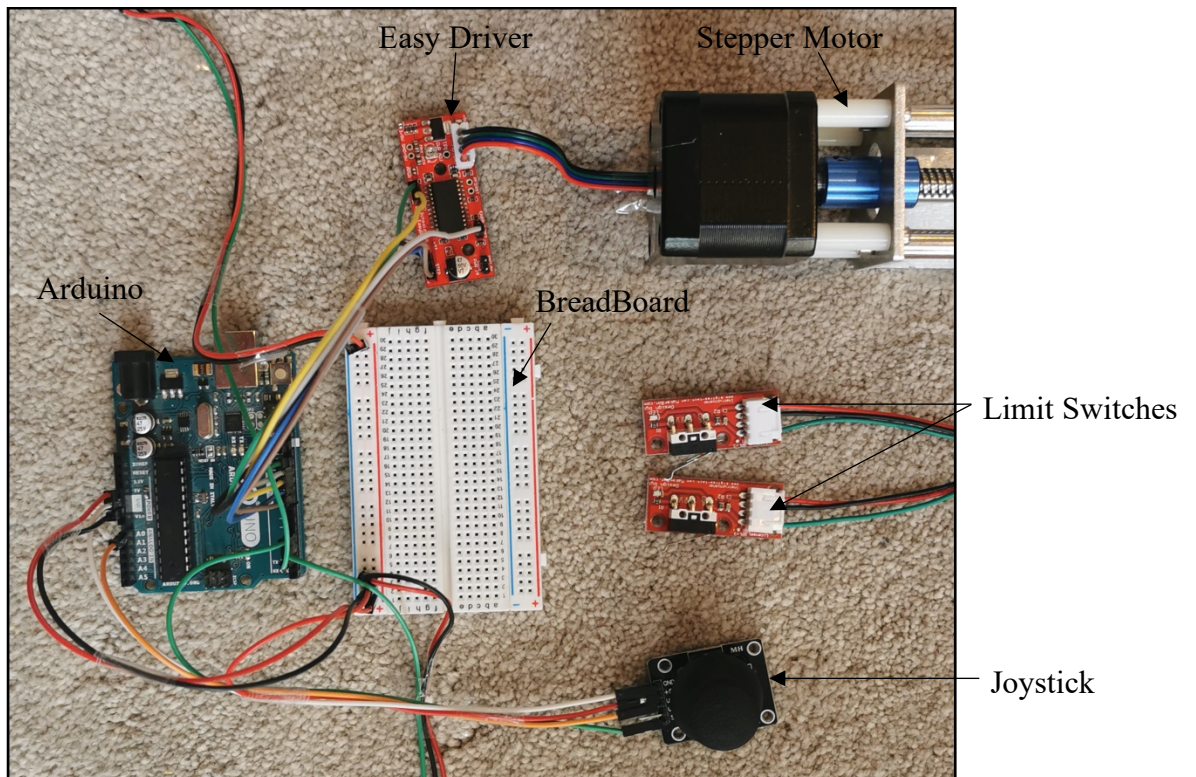


Figure 40: Actual setup of the electronic hardware that control the SP (without power supply).

A security system is required to not ‘over-compress’ or ‘un-compress’ the syringes too much, causing the plunger to leave the barrel (Fig41) or clash (Fig42). Limit switches are used to prevent that from happening. They are strategically placed at the front and the back of the SPM (Fig43). When pressed the motor stops immediately.

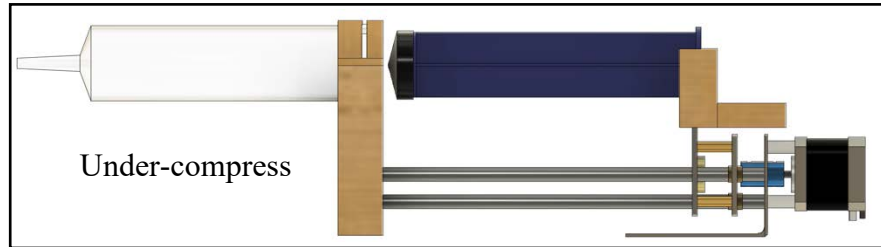


Figure 41: Left side view of the SPM when un-compressed too much.

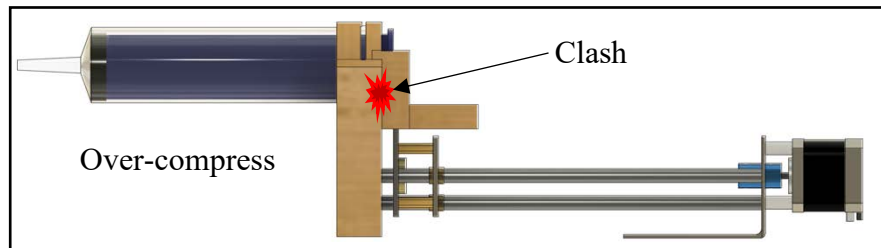


Figure 42: Left side view of the SPM when over compressed too much.

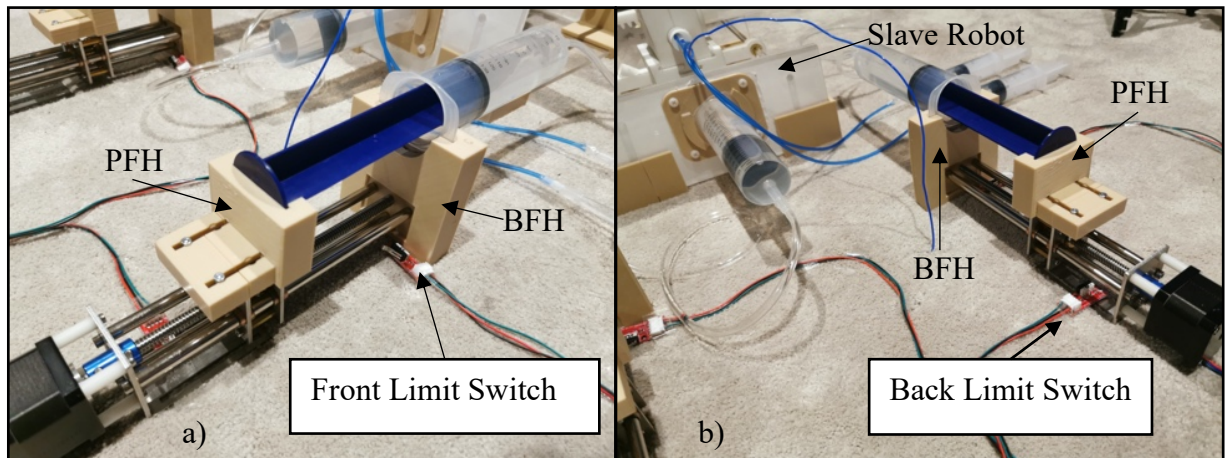


Figure 43: (a) Picture of the front switch that prevents an over-compression. (b) Picture of the switch that prevents the syringe to be ‘un-compress’ too much.

5.2.3 Code & Programming

The stepper motor is moved according to the analogue value of the X-axis of the joystick. 512 is centre, 0 is full left and 1023 is full right. If the analogue value is higher than 712 then a clockwise

rotation is generated, if the value is lower than 312, the motor rotates anti-clockwise. An arbitrary margin of plus or minus 200 in the analogue values from the centre was implemented before detecting a movement to prevent accidental or unwanted movement of the joystick by the interventionalist. It allows for better and smoother control of the catheter as the joystick is not too reactive. The status of the limit switches is then checked, if they are not activated, the motor is not stopped, else it is stopped. Finally, using the switch case function, the speed can be adjusted to three speed modes if the joystick is clicked (see section 10.3)(22).

6.0 Experimental Setup & Results

6.1 Original Experimental Setup

The original experimental setup should have been implemented in collaboration with another student named Shreya Patel. She designed a 3D model of the right ventricle of a heart obtained from the MRI scans of a 9 years-old female pediatric patient with pulmonary arterial hypertension (PAH) (Chapter 11.0). The model is sufficient for testing the right heart catheterisation, which has been considered the gold standard for diagnosing and monitoring disease progression in patients with PAH. A connector would then be attached to an inlet of a pump, such as the Harvard Apparatus Pulsatile Blood Pump (Fig44), to simulate the blood flow up through the Inferior Vena Cava (IVC) and into the right side of the heart. The catheter would be guided up the IVC, through the right side of the heart and into the pulmonary artery(Fig45).

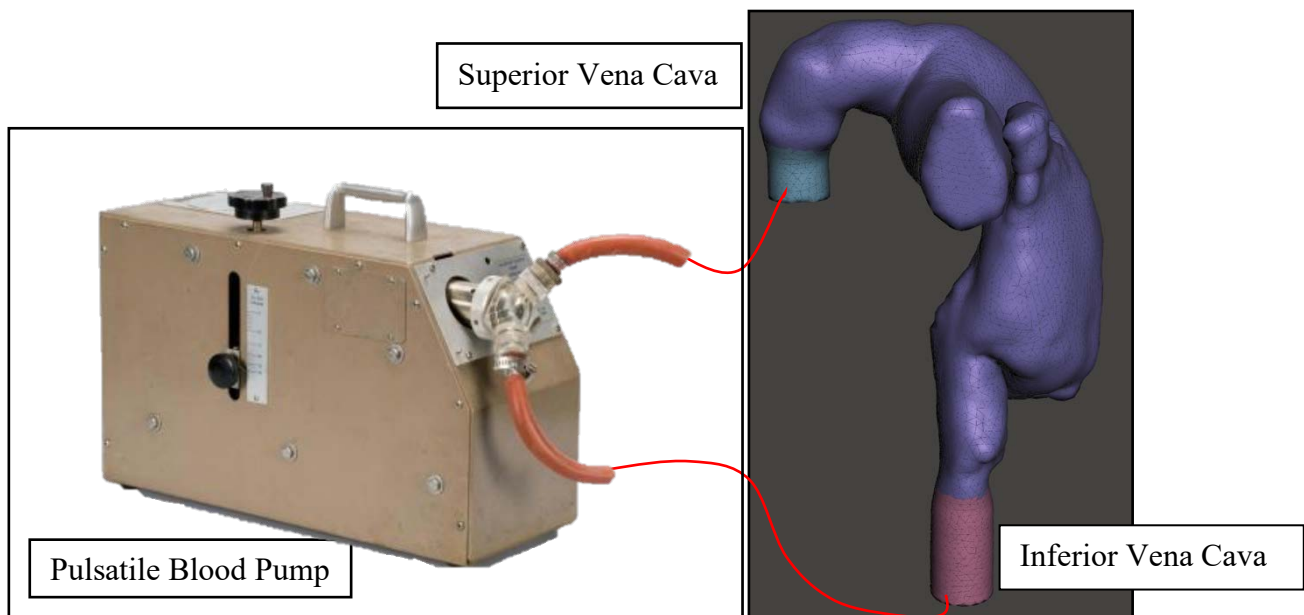


Figure 44: The side view makes it apparent that the right pulmonary artery and SVC have now been closed off. The blue section below the left pulmonary artery is also connector that has been added to facilitate attachment to the outlet of the mock circulatory system, as fluid would flow in through the IVC and out through the left pulmonary artery.

The setup required the master/slave robot as well as an MRI scanner from UCL hospital in which Shreya's design would have been placed. Using the master control system and long plastic tubes that connect the master to the slave robot, the intervention would have been done remotely. To see the catheter in the MRI scanner, a fluoroscopic dye or a fluoroscopic catheter tip would have been employed.

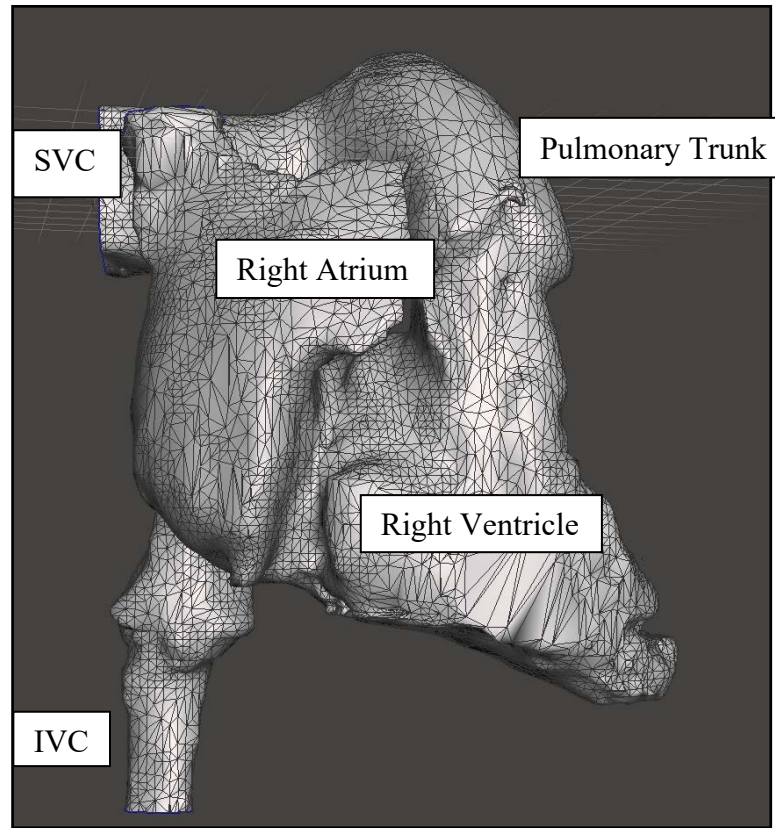


Figure 45: Front view of the 3D heart model. Blood would usually flow from the SVC and IVC into the right atrium, right ventricle and out through the pulmonary trunk.

6.2 Alternative Experimental Setup

The alternative experimental setup was designed to test the performance and understand the limitations of the slave robot. Unfortunately, the MRI scanner and the 3D model heart were not present^(*)(**). Nevertheless, different tests were designed to assess the resolution, agility and reactivity of the slave robot. The full set up can be seen on Fig46. Three SP were employed to actuate respectively the rotational, translational and compressive plates.

The setup can be divided into 6 different sections. In A, the two syringes actuating the compressive plates, in B the slave robot, in C the SP that actuates the RMM, in D the SP that actuates the LMM, in E the control system for the RMM and in F the control system for the LMM. In E and F, the Arduino boards are powered using 9V batteries and two additional 9V batteries are used to power the stepper motors. Finally, the catheter (Fig47) is replaced by a 2 mm diameter PLA filament*.

Note: (i) On Fig46, the SP in C and D are very close to the slave robot for aesthetic reasons, however, in a real-life situation, they should be more than 5m apart. (ii) Since the tee connectors could not be obtained*, the compressive plates are actuated manually using two syringes, so the third syringe pump is not used (A in Fig46).

*Because of the COVID-19 situation.

**MRI scanner and the catheter could not be acquired. Plus, Shreya was not able to print her heart and the hospital was not accessible.

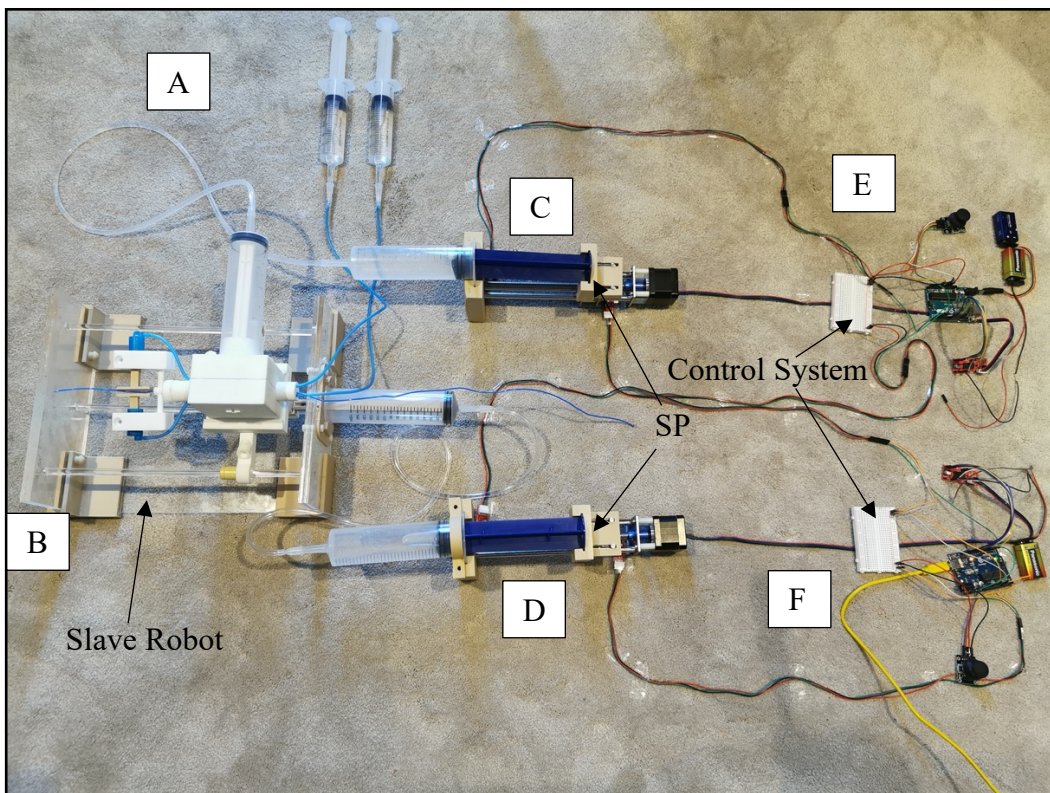


Figure 46: Picture from above of the alternative experimental setup.

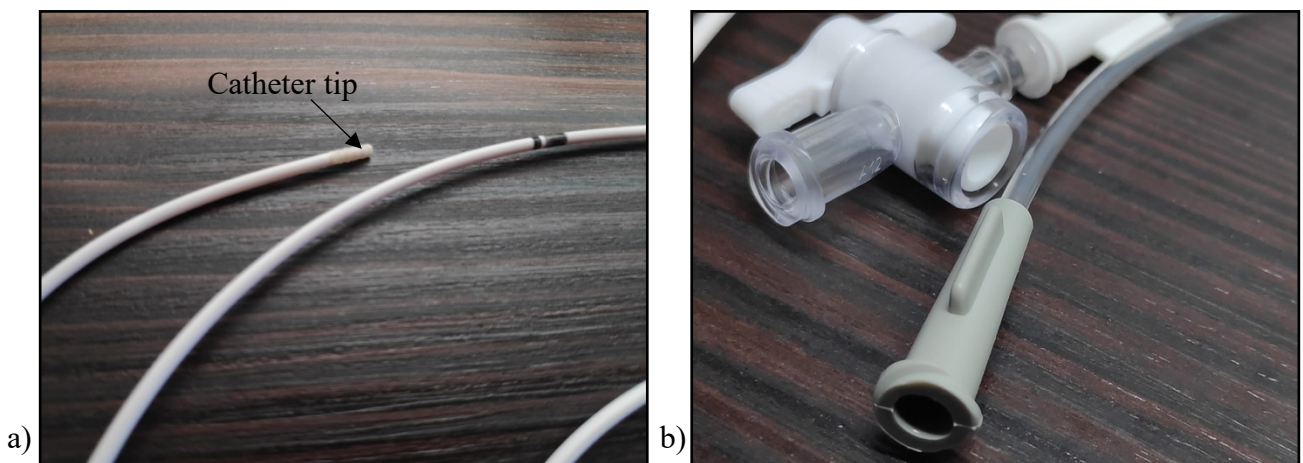


Figure 47: (a) Catheter tip view from above. (b) Detailed view of one of the catheter insertion part.

6.4 Protocol

6.4.1 Experiment 1

The first experiment evaluated the ability of the RMM to rotate a 2mm catheter. The SP in C is actuated using the control system in E and a picture was taken each time the SP displaced a volume of water equivalent to 10ml (Fig46). To recognize the catheter's rotation, a small piece of yellow tape was attached to its tip indicating its direction. Fig48,49 demonstrate that the RMM can rotate the catheter.

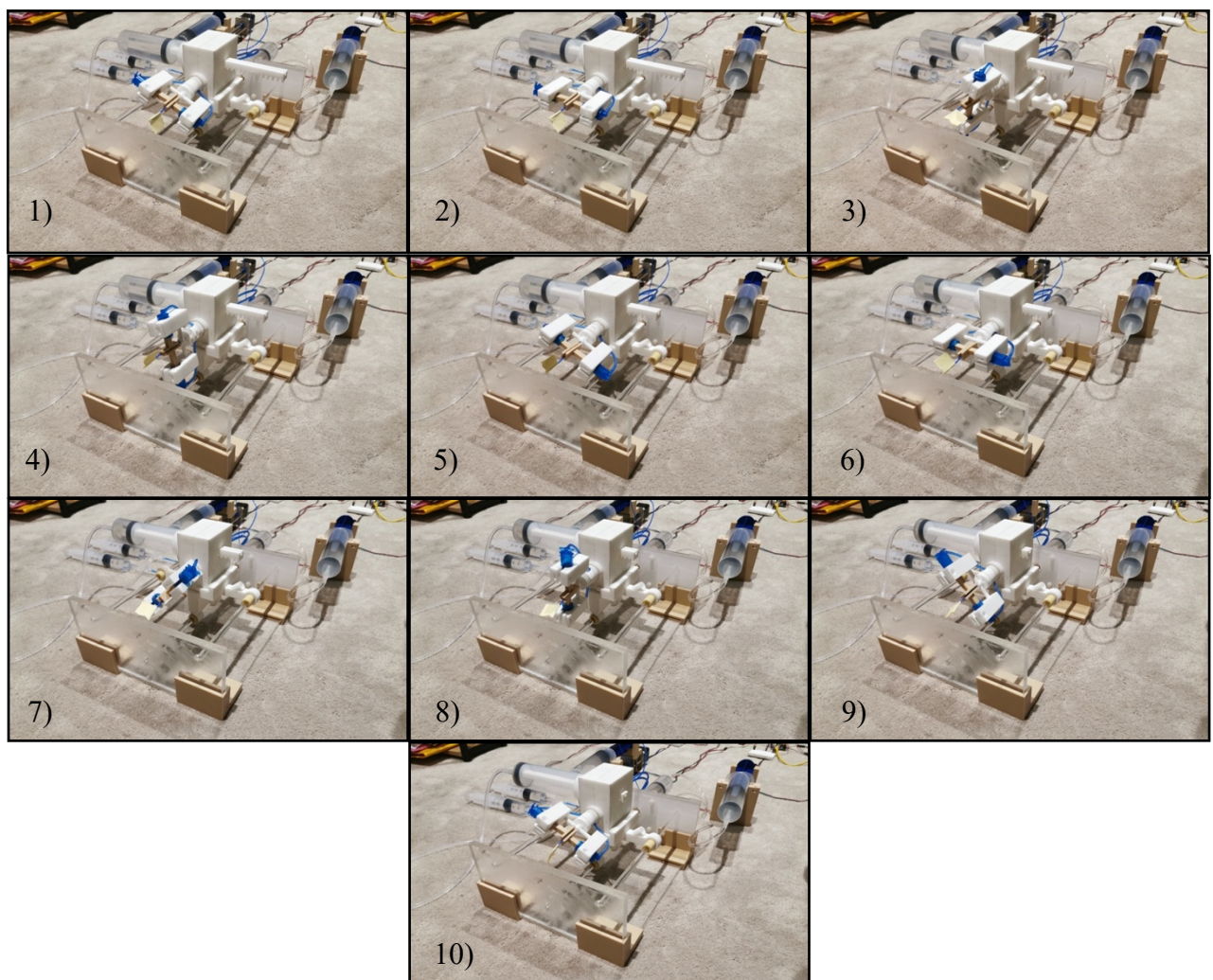


Figure 48: Continuous shooting from the front right corner of RMM being actuated by the SP.

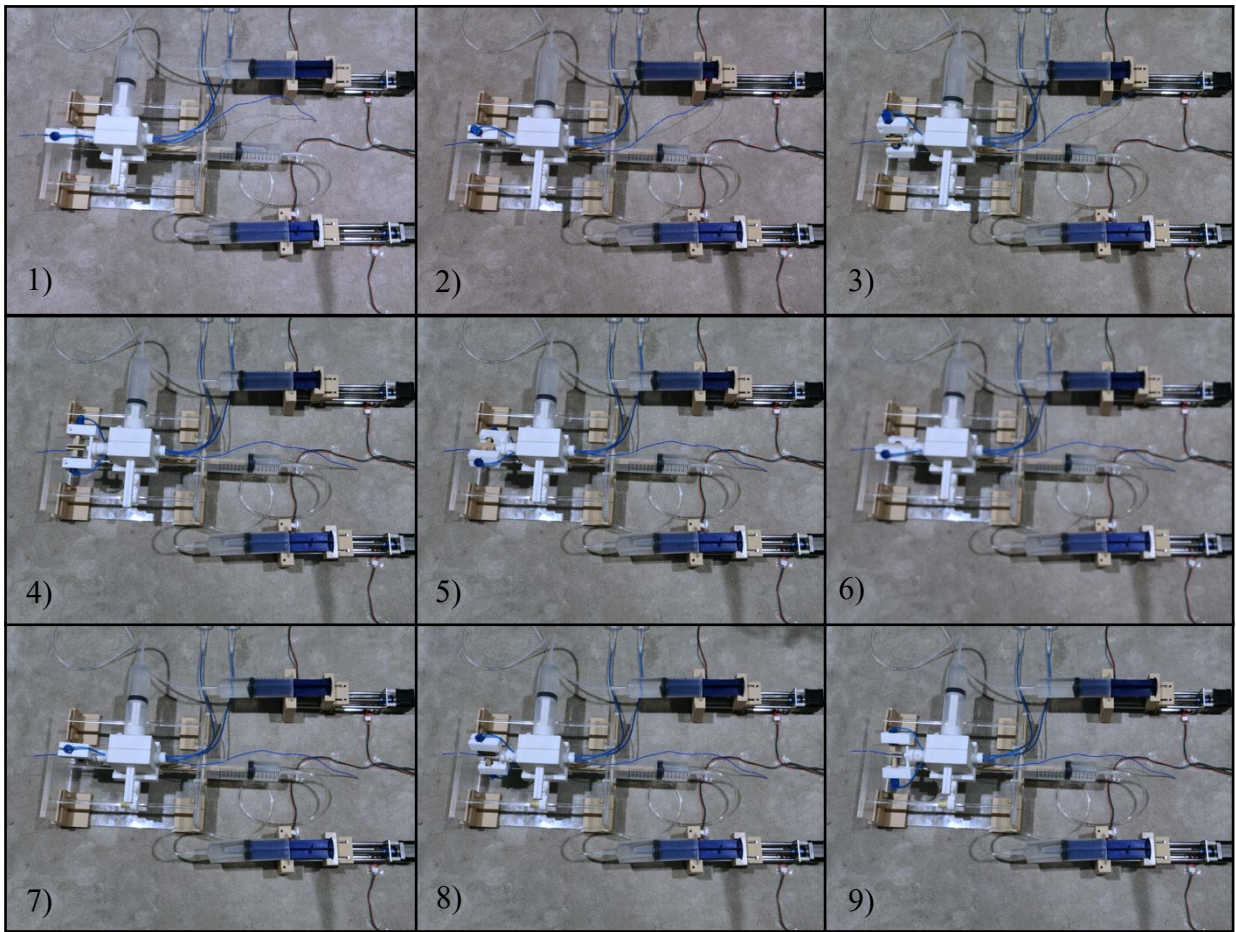


Figure 49: Continuous shooting from above of the RMM being actuated by the SP.

6.4.2 Experiment 2

In the second experiment, the same approach was followed with the LMM, the process is displayed in Fig50,51. The LMM is able to move the catheter translationally.

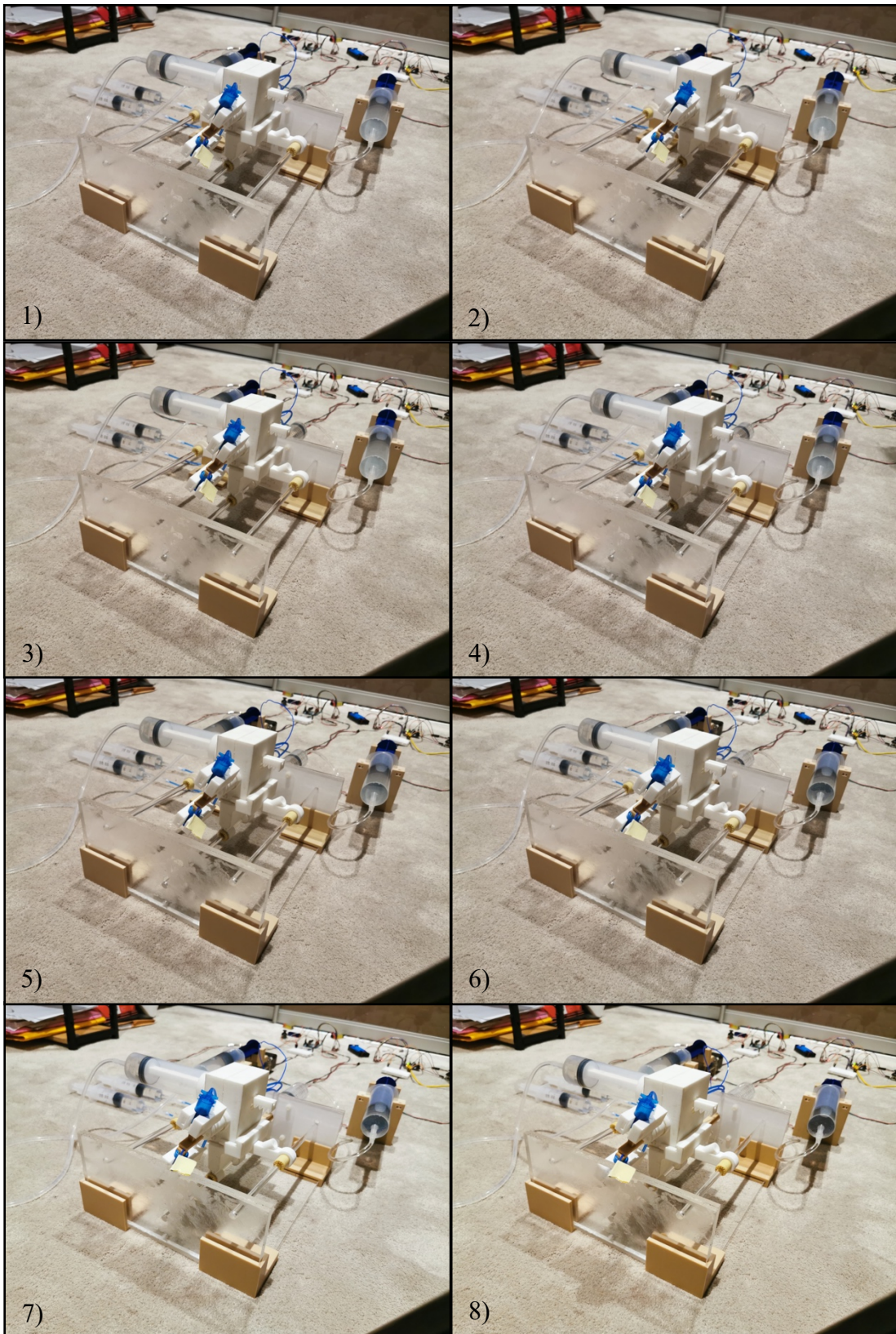


Figure 50: Continuous shooting from the front right corner of the LMM being actuated by the SP.

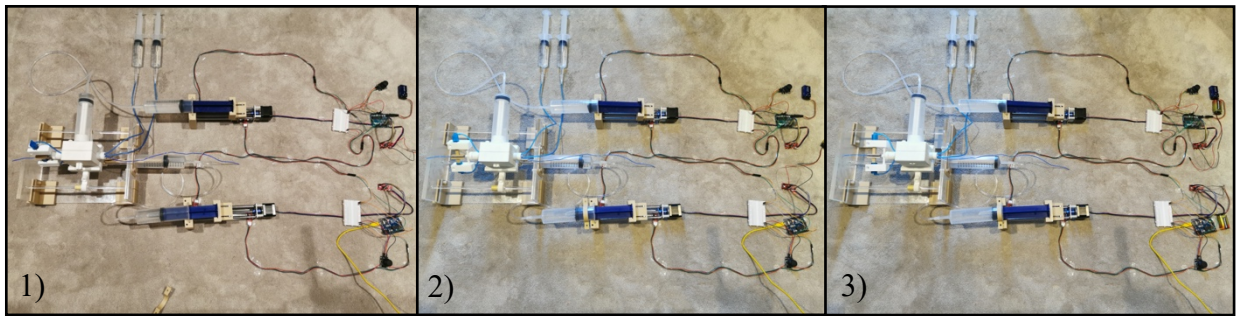


Figure 51: Continuous shooting above of the LMM being actuated by the SP.

6.4.3 Experiment 3

The third experiment evaluated the ability of the slave robot to simultaneously rotate and move the catheter translationally, the process is displayed on Fig52.

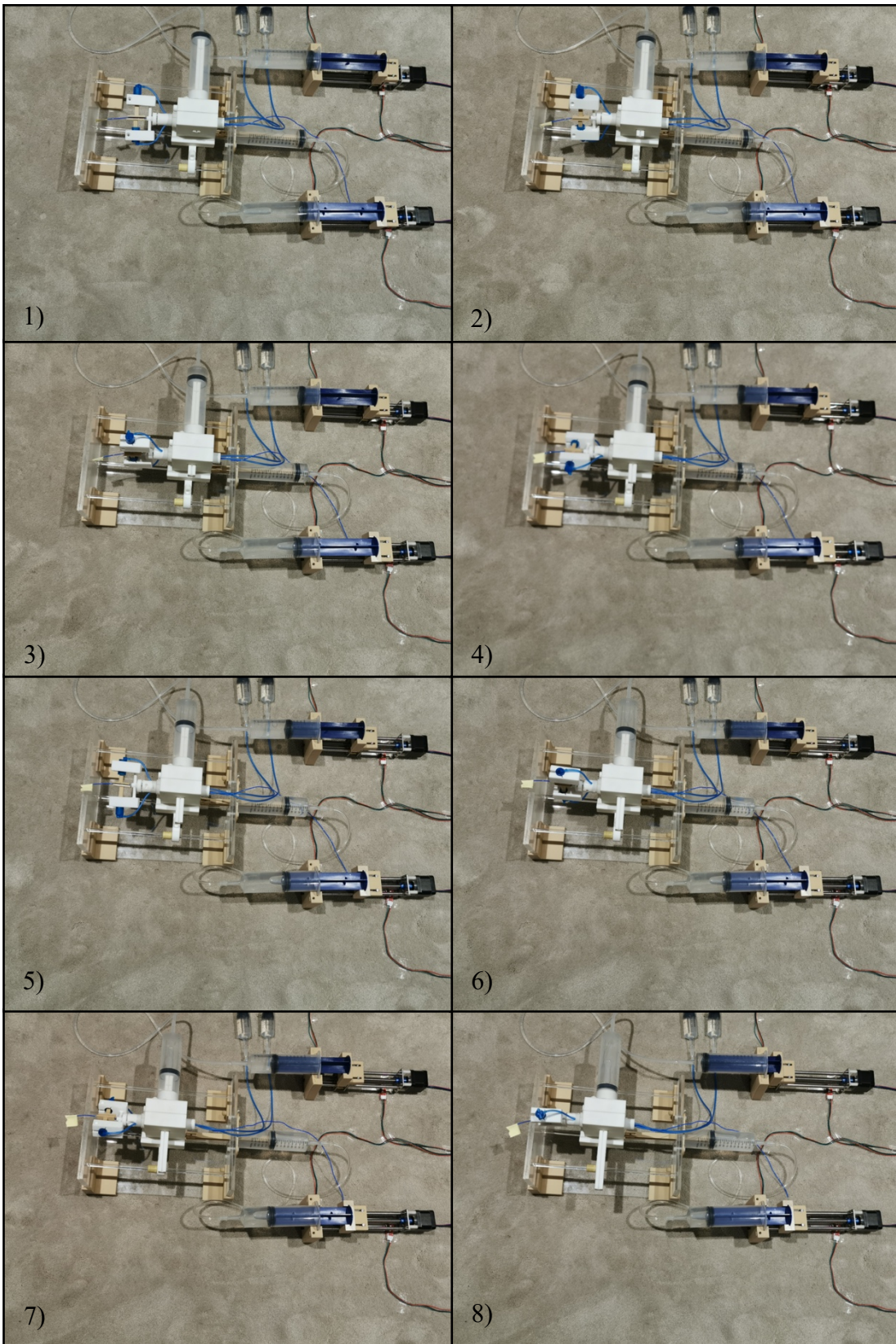


Figure 52: Continuous shooting from above of the RMM and LMM being actuated together by the two SP.

6.5 Measurements

During these experiments, data regarding the resolution, accuracy, reactivity and velocity of the slave robot was collected and are reported in the following tables:

1. Table 2 reports the backlash delay which represents the time difference between the actuation of the SP and initial motion of the LGR.
2. Table 3 reports the span of motion of the plunger in the syringe pump compared to the span of motion of the LGR for different distances. Both measurements were done over 5 trials.
3. Table 4 reports the average speed of the LGR when actuated with the four different speed modes (V1 the maximum speed achievable, V4 is the smallest possible speed achievable).
4. Table 5 reports the backlash delay representing the time difference between the actuation of the SP and the initial motion of the LMM.
5. Table 6 reports the average speed of the LMM when actuated with the four different speed modes.

Trial	Backlash delay (s) (LGR)
1	0.63
2	0.65
3	0.50
4	0.85
5	0.46

Table 2: Report of the backlash delay between the SP and the LGR for 5 different trials.

Trials	Syringe pump span of motion (mm)	LGR in RMM span of motion (mm)
1	112	113
2	100	101
3	70	70
4	40	39
5	10	8

Table 3: Comparison of the span of motion of the plunger in the SP compare to the span of motion of the LGR for different distance.

Speed chosen on the program.	Time to expand the LGR from a non-extended position to the maximum possible extension (112mm). (Average on 5 trials)	Speed of the LGR in mm/s	Equivalent Angular velocity of the RSH (rad/s)
V1	121.18	0.92	0.07
V2	36.99	3.03	0.22
V3	14.03	7.98	0.58
V4	2452.8	0.04	0.003

Table 4: Average speed of the LGR when actuated with the different speed modes.

Trial	Backlash delay (s) (LMM)
1	0.76
2	0.66
3	0.67
4	0.38
5	0.52

Table 5: Report of the backlash delay between the SP and the LMM for 5 different trials.

Speed chosen on the program.	Time to expand the LMM from a non-extended position to the maximum possible extension (93mm). (Average on 5 trials)	Speed of the LGS in mm/s
V1	97.52	0.95
V2	29.60	3.14
V3	11.20	8.30
V4	2036.70	0.04

Table 6: Average speed of the LMM when actuated with the different speed modes.

6.6 Results

Table 2 and 5 show that the backlash delay is very small ($< 1\text{s}$), demonstrating a good reactivity of the slave robot. In practice, the use of 5m plastic tubes might increase that delay slightly. Table 3 demonstrates the precision and accuracy of control. Indeed, both the SP and the LGR are moving simultaneously. The minor differences ($< 5\text{mm}$) are due to the fact that the LGR do not stop immediately when the SP stops. The inertia acquired by the LGR makes it stop a little after the SP. Finally, Table 4 and 6 indicate that the slave robot can be used for accurate positioning as it can move at extremely low speed (0.04mm/s) and rotate the catheter at equally slow angular velocity (0.003 rad/s), adequate for precise positioning in the heart ventricle. However, it is also able to move at a faster speed ($\approx 8\text{mm/s}$) and angular velocity (0.58 rad/s), more suitable for motion of the catheter in arteries.

7.0 Discussion

7.1 Limitations and Improvements

7.1.2 Batteries

First, the stepper motors are rapidly consuming the 9V batteries. To save the batteries life, the Arduino in F was powered using a computer (Fig46). This can be dangerous when performing a cardiac catheterisation, thus, more appropriate batteries should be used with a better longevity. An alternative would be to use a an alternative stepper motor driver that can support higher voltages and can precisely regulate the current. It can then be connected to reliable power supply such as a wall socket.

7.1.3 Rotational Motion Mechanism

In experiment 1, the catheter was slipping a little when the RMM was actuated. Not enough pressure was applied by the compressive plates, so the catheter was not secured. The pressure could be easily increased by actuating the syringes in A (Fig46); however, this can deform and damage the catheter. Alternatively, the friction force could be increased. Indeed, the compressive plates are made of PLA and the catheter is also in PLA (in that situation), therefore, the friction factor is very low. Small pieces of rubber could be attached to the compressive plates to increase the friction (D on Fig53). The small piece of rubber could not be obtained, so the friction force was increased by increasing the compressive force (Fig48,49). The friction force only depends on the compressive force and the friction factor, therefore, the alternative solution with the rubber pieces would have been an appropriate improvement to the slave robot.

7.1.4 Linear Motion Mechanism

Friction is not an issue when the catheter is moved translationally. Indeed, when rotating the catheter, the torsional forces counteract the rotation and need to be overcome. However, when moving the catheter translationally, those forces are not present and therefore, the friction force does not need to be increased.

However, friction between the catheter and the shaft hole caused the catheter to move slightly backward, when the LMM was going backward, even though the catheter was not constricted within the compressive plates. When the LMM travelled a distance of 100 mm backward, the catheter went 17 mm backward. Although not significant, for accurate manipulation, the catheter should not have moved at all (when it is not grabbed). This inevitable friction between the catheter and the shaft cannot be avoided. Therefore, an alternative design of the RSH was devised (Fig53).

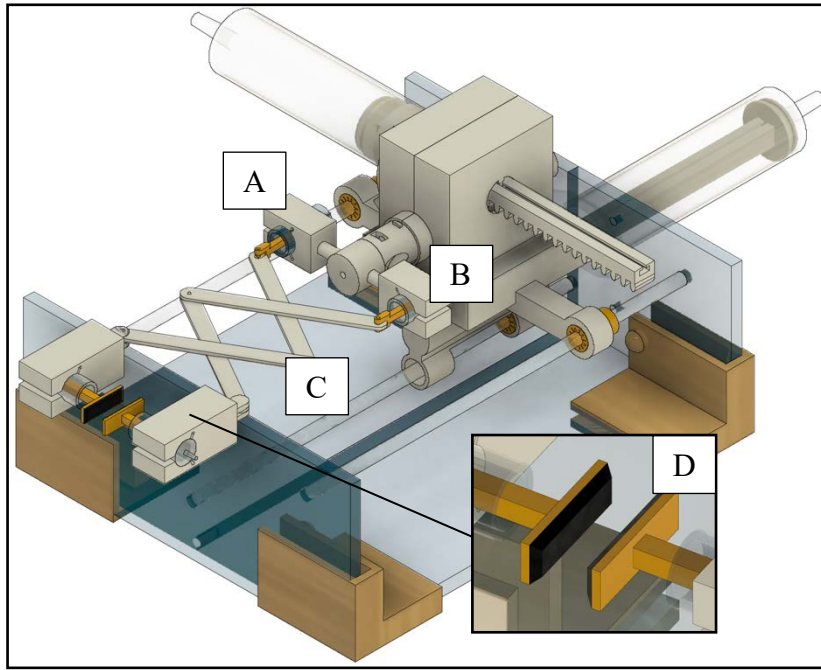


Figure 53: FRCV of the alternative RSH assembled on the slave robot.

The new RSH possesses two additional syringes (A and B on Fig53) as well as a new mechanism that allows to vary the distance of the compressive plates relative to the shaft (C). This new version of the RSH was designed so that it is the only piece that needs to be re-printed and it can fit on the existing shaft using the same connector piece of Fig10a. This mechanism allows to move the LMM backward without moving the catheter backward (Fig54).

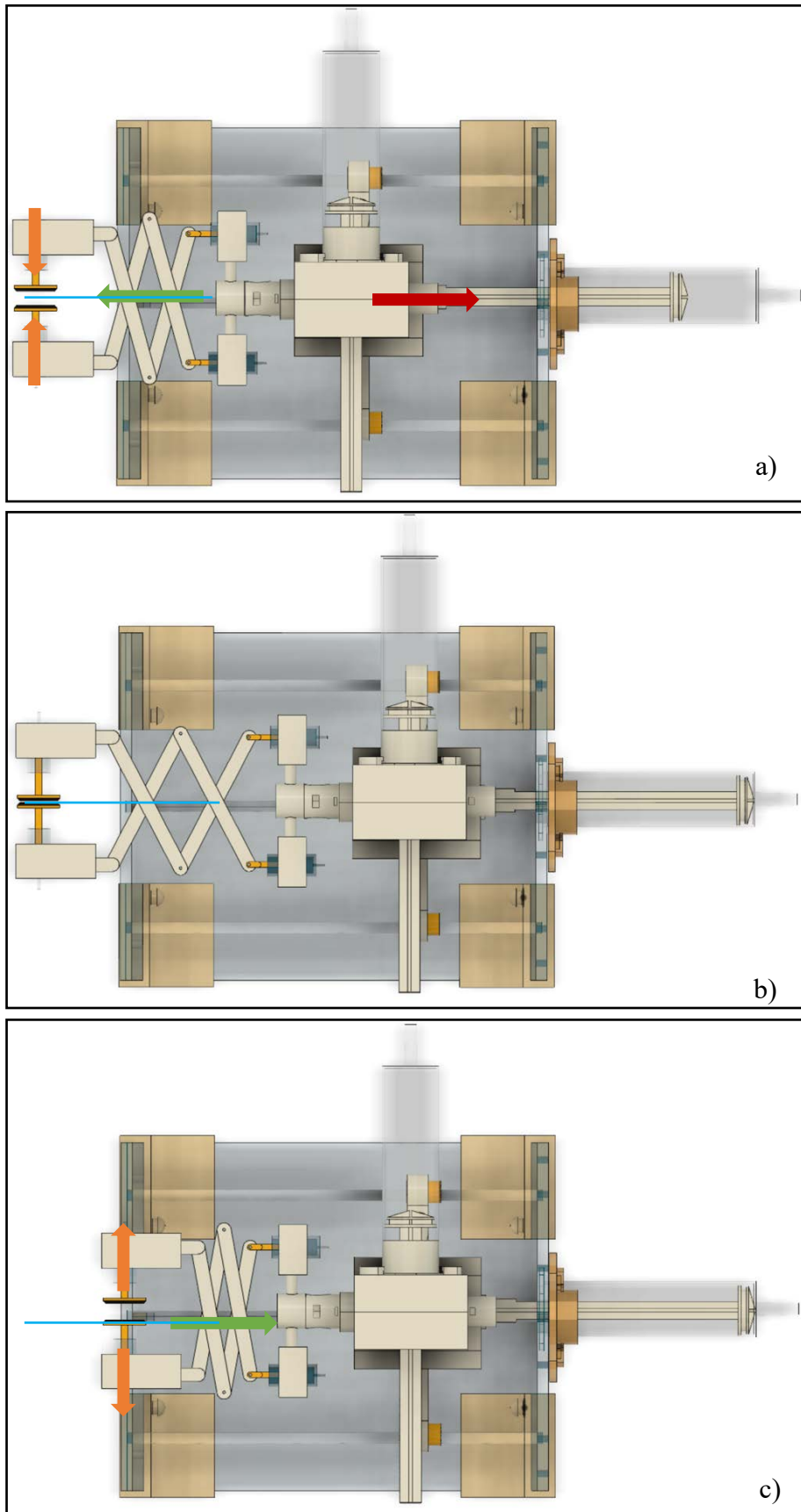


Figure 54: Illustration of the new RSH that prevents the catheter from moving backward with the LMM. The orange arrows represent the actuation of the compressive plates, the green one represents the actuation of the new RSH and the red one represents the actuation of the LMM. The catheter is represented with a blue line.

Following the steps illustrated above allows moving the LMM backwards only, without moving the catheter. The first step consists of grabbing the catheter with the compressive plates, then moving the LMM backwards and at the same time extending proportionally the new RSH. If those actions are done simultaneously, the catheter remains still (Fig54b). The final step is a simple retraction of the new RSH (Fig54c). This new RSH also allows moving the catheter translationally (Fig55). Thus, the existing LMM is not required anymore. Also, it requires four tubes to go inside the shaft to actuate the four syringes, which is not a problem (Fig56). Certainly, these improvements would need to be tested to prove their efficacy.

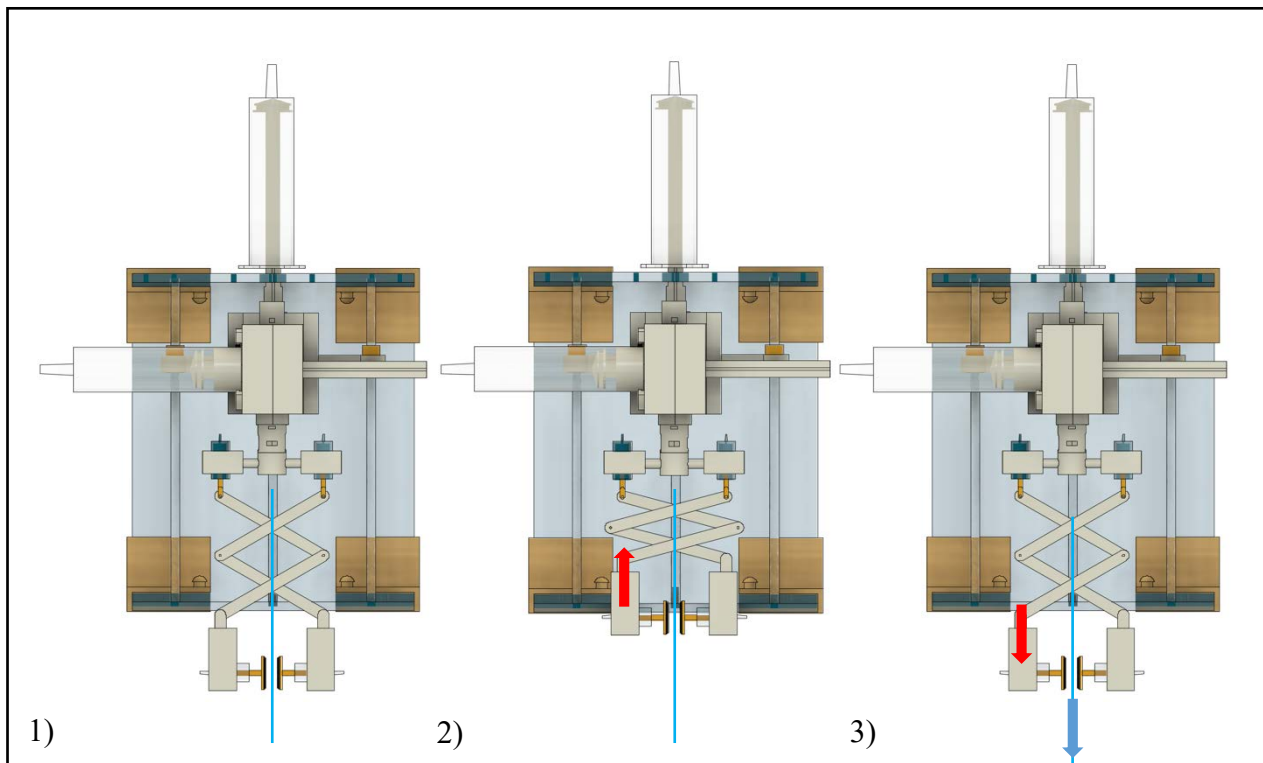


Figure 55: Use of the RSH as an alternative LMM



Figure 56: Picture of the shaft with the four tubes for the alternative RSH.

8.0 Conclusion & Future Work

8.1 Conclusion

After comparing the results to the project aims, it can be stated that all the key criteria for the MRI compatible robot have been met. A remotely controlled MRI safe master/slave robot that can steer a catheter in 2 DOF at a time has been developed, assembled and successfully tested. The robot fulfils the MR Safe standard (ASTM F2503-13)(2).

8.2 Future work

Nevertheless, the master and slave robots have several limitations, which have highlighted multiple areas of improvement procuring the model more accuracy, control and dexterity. The next steps would be to:

- Implement the improvements stated in section 7.1 and test the master/slave robot in a real-life situation.
- Improve the syringe actuation unit to more modern pneumatic actuators in line with Lee et al. works (2).
- Re-design the control system to a more intuitive and compact one, similar to the one developed by Tavallaei et al., and implement haptic feedback. (4).

9.0 References

1. Abdelaziz MEMK, Stramigioli S, Yang G-Z, Kundrat D, Pupillo M, Dagnino G, et al. Toward a Versatile Robotic Platform for Fluoroscopy and MRI-Guided Endovascular Interventions: A Pre-Clinical Study. In Institute of Electrical and Electronics Engineers (IEEE); 2020. p. 5411–8.
2. Lee KH, Fu KCD, Guo Z, Dong Z, Leong MCW, Cheung CL, et al. MR Safe Robotic Manipulator for MRI-Guided Intracardiac Catheterization. *IEEE/ASME Trans Mechatronics*. 2018 Apr 1;23(2):586–95.
3. Groenhuis V, Siepel FJ, Veltman J, van Zandwijk JK, Stramigioli S. Stormram 4: An MR Safe Robotic System for Breast Biopsy. *Ann Biomed Eng [Internet]*. 2018 Oct 15 [cited 2020 Mar 20];46(10):1686–96. Available from: <http://www.ncbi.nlm.nih.gov/pubmed/29786775>
4. Tavallaei MA, Thakur Y, Haider S, Drangova M. A magnetic-resonance-imaging-compatible remote catheter navigation system. *IEEE Trans Biomed Eng*. 2013;60(4):899–905.
5. Susil RC, Yeung CJ, Halperin HR, Lardo AC, Atalar E. Multifunctional interventional devices for MRI: A combined electrophysiology/MRI catheter. *Magn Reson Med [Internet]*. 2002 Mar 1 [cited 2020 Mar 24];47(3):594–600. Available from: <http://doi.wiley.com/10.1002/mrm.10088>
6. Razavi R, Hill DL, Keevil SF, Miquel ME, Muthurangu V, Hegde S, et al. Cardiac catheterisation guided by MRI in children and adults with congenital heart disease. *Lancet [Internet]*. 2003 [cited 2020 Mar 24];362:1877–82. Available from: www.thelancet.com
7. Nayak KS, Cunningham CH, Santos JM, Pauly JM. Real-Time Cardiac MRI at 3 Tesla. *Magn Reson Med*. 2004;51(4):655–60.
8. Uecker M, Zhang S, Frahm J. Nonlinear inverse reconstruction for real-time MRI of the human heart using undersampled radial FLASH. *Magn Reson Med*. 2010;63(6):1456–62.
9. Hempel E, Fischer H, Gumb L, Höhn T, Krause H, Voges U, et al. An MRI-compatible surgical robot for precise radiological interventions. *Comput Aided Surg*. 2003;8(4):180–91.
10. Chinzei K, Miller K. Towards MRI guided surgical manipulator. *Med Sci Monit*. 2001;7(1):153–63.
11. Chinzei K, Kikinis R, Jolesz FA. MR compatibility of mechatronic devices: Design criteria. *Lect Notes Comput Sci (including Subser Lect Notes Artif Intell Lect Notes*

- Bioinformatics). 1999;1679:1020–31.
- 12. Payne CJ, Rafii-Tari H, Yang GZ. A force feedback system for endovascular catheterisation. In: IEEE International Conference on Intelligent Robots and Systems. 2012. p. 1298–304.
 - 13. Rafii-Tari H, Payne CJ, Yang GZ. Current and emerging robot-assisted endovascular catheterization technologies: A review. *Ann Biomed Eng*. 2014;42(4):697–715.
 - 14. Dagnino G, Liu J, Abdelaziz MEMK, Chi W, Riga C, Yang GZ. Haptic Feedback and Dynamic Active Constraints for Robot-Assisted Endovascular Catheterization. In: IEEE International Conference on Intelligent Robots and Systems. Institute of Electrical and Electronics Engineers Inc.; 2018. p. 1770–5.
 - 15. L. Di Biase, Y. Wang, R. Horton, G. Gallinghouse, P. Mohanty, J. Sanchez DP, M. Dare, R. Canby, L. Price, J. Zagrodzky, S. Bailey, J. Burkhardt and AN. Ablation of atrial fibrillation utilizing robotic catheter navigation in comparison to manual navigation and ablation: Single-center experience. *J Cardiovasc electro- Physiol*. 2009;20:1328–35.
 - 16. H. Ra i-Tari, C. Riga, C. Payne, M. Hamady, N. Cheshire, C. Bicknell and G-ZY. Reducing contact forces in the arch and supra-aortic vessels using the magellan robot. *J Vasc Surg*. 2015;64.
 - 17. Z. Shaikh, M. Eilenberg and TC. The amigo remote catheter system: From concept to bedside. *J Innov Card Rhythm Manag*. 2017;8:2795–802.
 - 18. Ernst S, Ouyang F, Linder C, Hertting K, Stahl F, Chun J, et al. Initial Experience with Remote Catheter Ablation Using a Novel Magnetic Navigation System: Magnetic Remote Catheter Ablation. *Circulation*. 2004;109(12):1472–5.
 - 19. C. Chautems and B. J. Nelson. The tethered magnet: Force and 5-dof pose control for cardiac ablation. 2017;4837–42.
 - 20. T. Patel, S. Shah and SP. Long distance tele-robotic-assisted percutaneous coronary intervention: A report of first-in-human experience. *EClinicalMedicine*. 2019;14:53–8.
 - 21. Whitney JP, Chen T, Mars J, Hodgins JK. A hybrid hydrostatic transmission and human-safe haptic telepresence robot. In: Proceedings - IEEE International Conference on Robotics and Automation. Institute of Electrical and Electronics Engineers Inc.; 2016. p. 690–5.
 - 22. Arduino NEMA stepper control with Joystick and Limit Switches – Brainy-Bits [Internet]. [cited 2020 May 13]. Available from: <https://www.brainy-bits.com/stepper-motor-with-joystick-and-limit-switches/>

10.0 Appendix

10.1 Additional Resources

10.1.1 Syringe Description

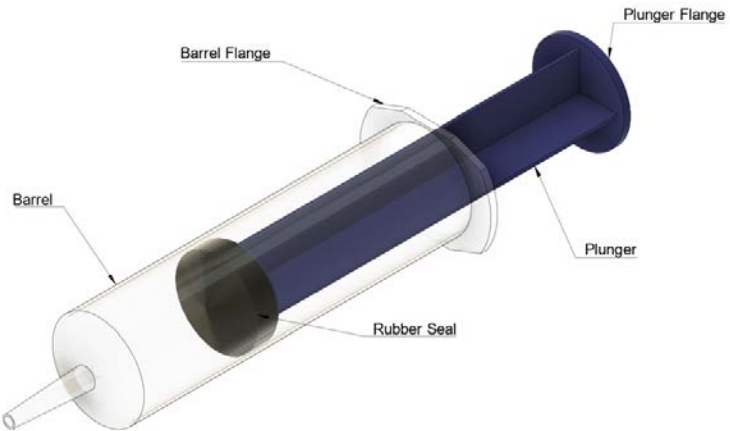


Figure 57: Description of the different syringe parts.

10.1.2 Linear Syringe Pump

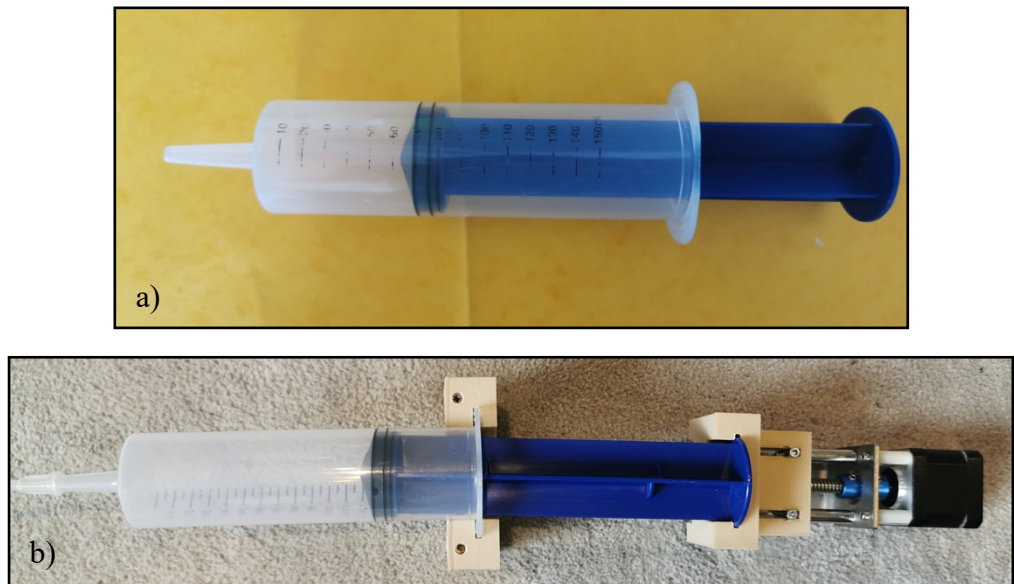


Figure 58: a) Picture of the syringes used for the syringe pumps. b) Top picture of the syringe pump mechanism

10.1.3 MR Compatibility

Magnetic Resonance (MR) compatibility has been a tough hurdle for device and mechatronic developers. Shellock intensively studied this subject and issued a guidebook on the compatibility of several medical devices. Schenk defined MR compatibility and classified numerous materials. New standards have been introduced to avoid confusion and errors originating from previous terminology (MR compatible / MR safe), which are no longer used in new research. The ASTM F 2503 standards defines three possible classifications for MRI devices:

- MR safe: device that contains exclusively non-metallic, non-magnetic and non-conductive materials, and can be based on a scientific rationale (i.e.: material composition) rather than test data. Then states that a foreign device is MR safe when it does not add risk to human or any equipment by placing it in the MR environment, however, it may affect imaging quality.
- MR conditional: are only safe when used under certain tested conditions,
- MR unsafe: are known to pose hazards in MRI environments.

10.2 Evolution of The Master/Slave Components

10.2.1 Shaft

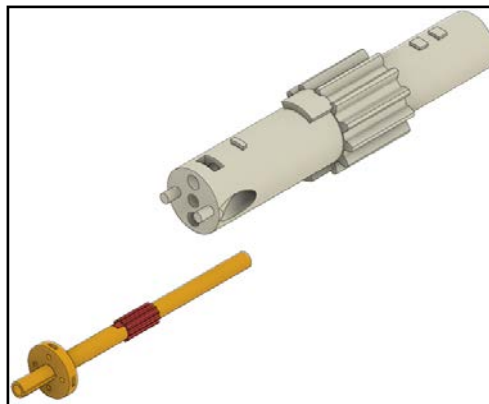


Figure 59: CAD models comparing the initial shaft design to the current rod design.



Figure 60: PLA 3D print of the initial version of the current shaft design. PLA was not suitable for this component.

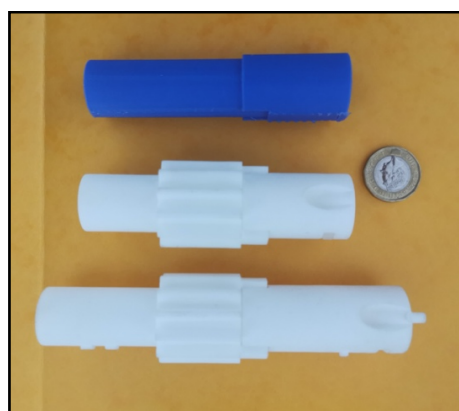


Figure 61 : From top to bottom, the evolution of the shaft component. The bottom one represents the current one and the middle one represents a former version (without stoppers on its surface).

10.2.2 Linear Rack



Figure 62: Different version of the LGR component.

10.2.3 Casing

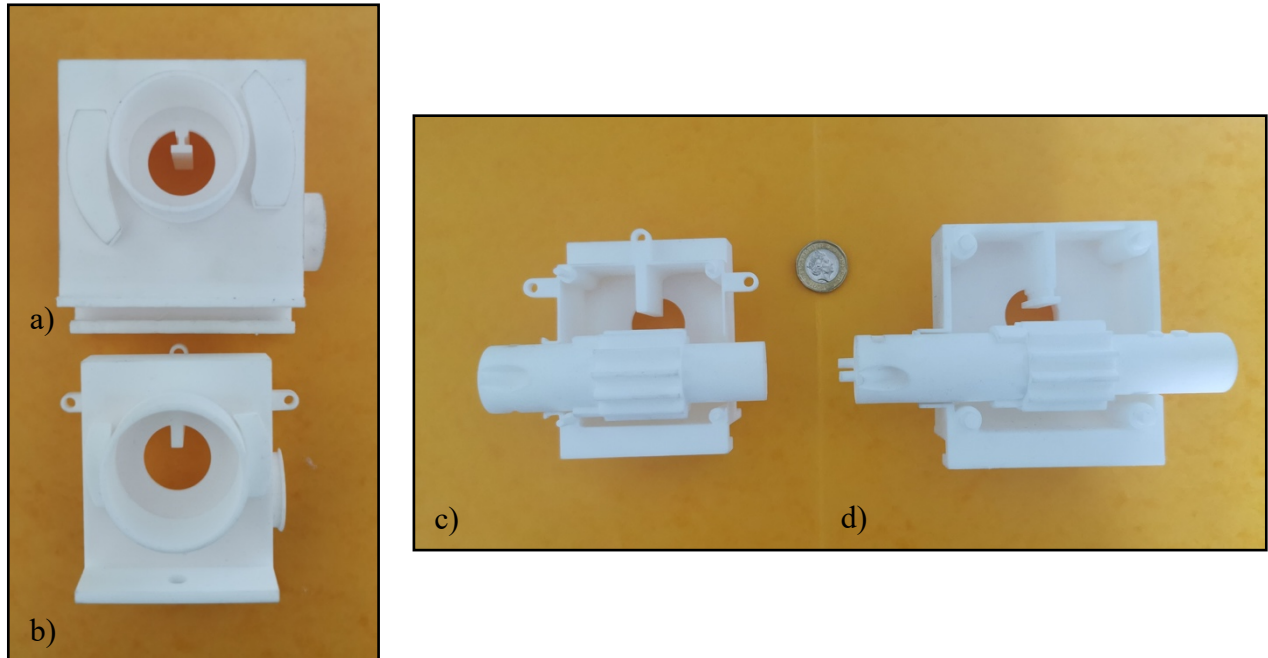


Figure 63: a) Picture of the current version of the casing. b) Picture of the old version of the casing. c) Picture of the old version of the casing with the former version of the shaft. d) Picture of the current shaft and casing.

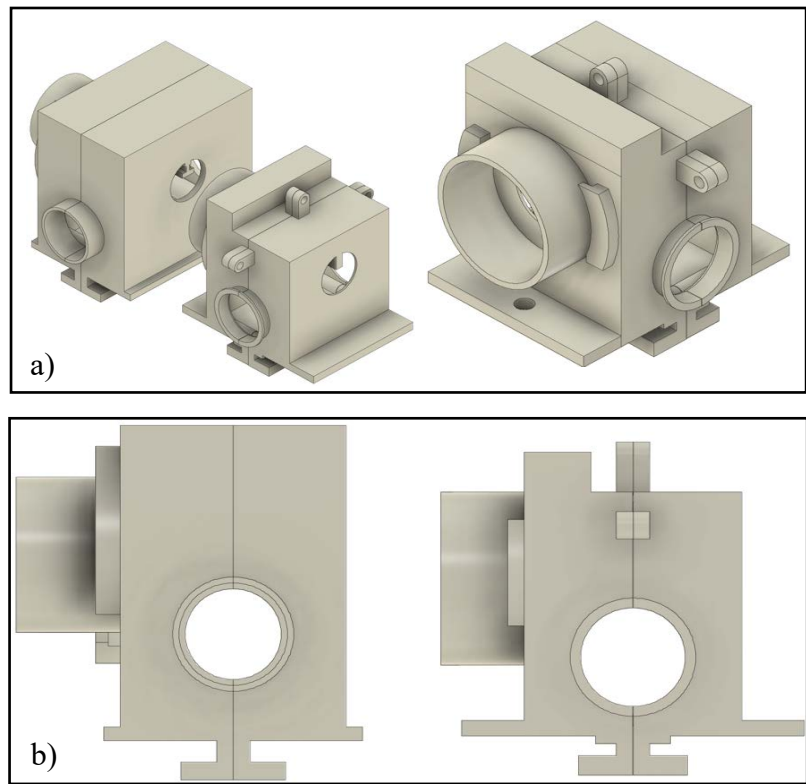


Figure 64: a) On the left, a FRCV of the different version of the casing. On the right, a FRCV of the former version of the casing.
 b) Front view of the different version of the casing (current version on the left).

10.2.4 Syringe Holder Mechanism

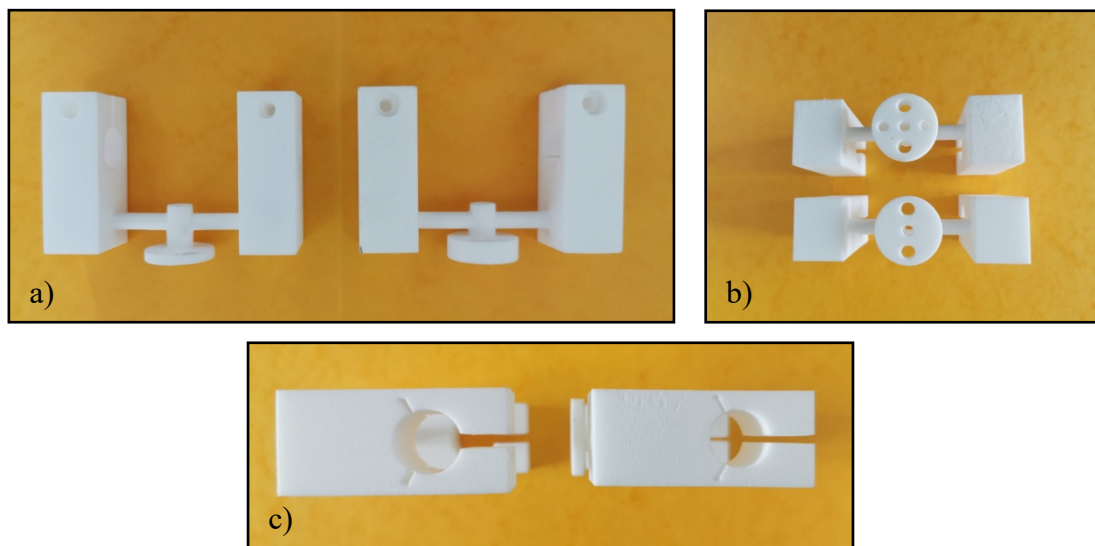


Figure 65: a) Picture of the different version of the RSH (current version on the left). b) Picture of the different connector piece used for the RSH (current version on top). c) Picture of the different version of the holes in the RSH (current version on the left).

10.2.5 Compressive Plates

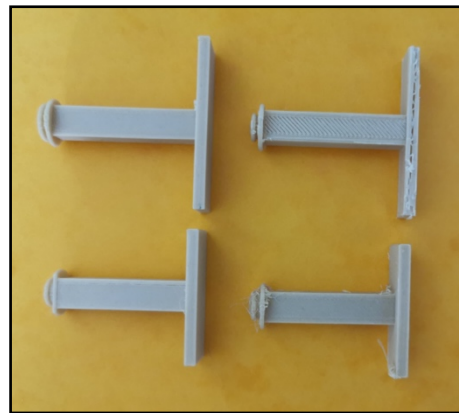


Figure 66: Different version of the compressive plates (current one : Top-left).

10.2.6 Alternative Linear Motion Mechanism

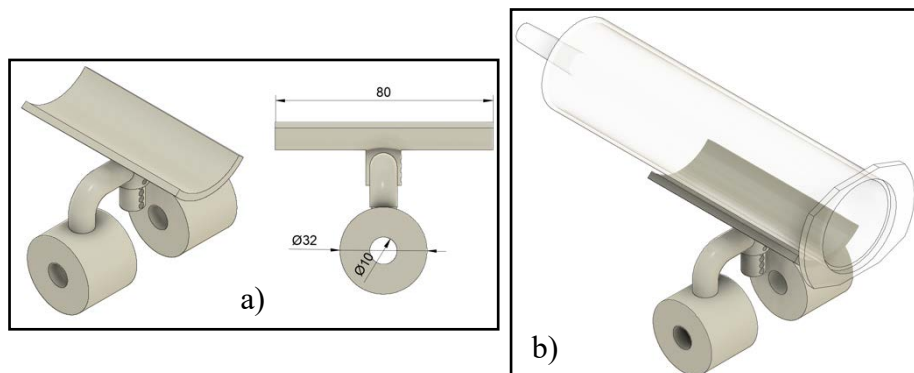


Figure 67: a) Support syringe slider that is used to support the weight of the syringe used for the rotating mechanism. b) Representation of the support syringe slider with the syringe on it.

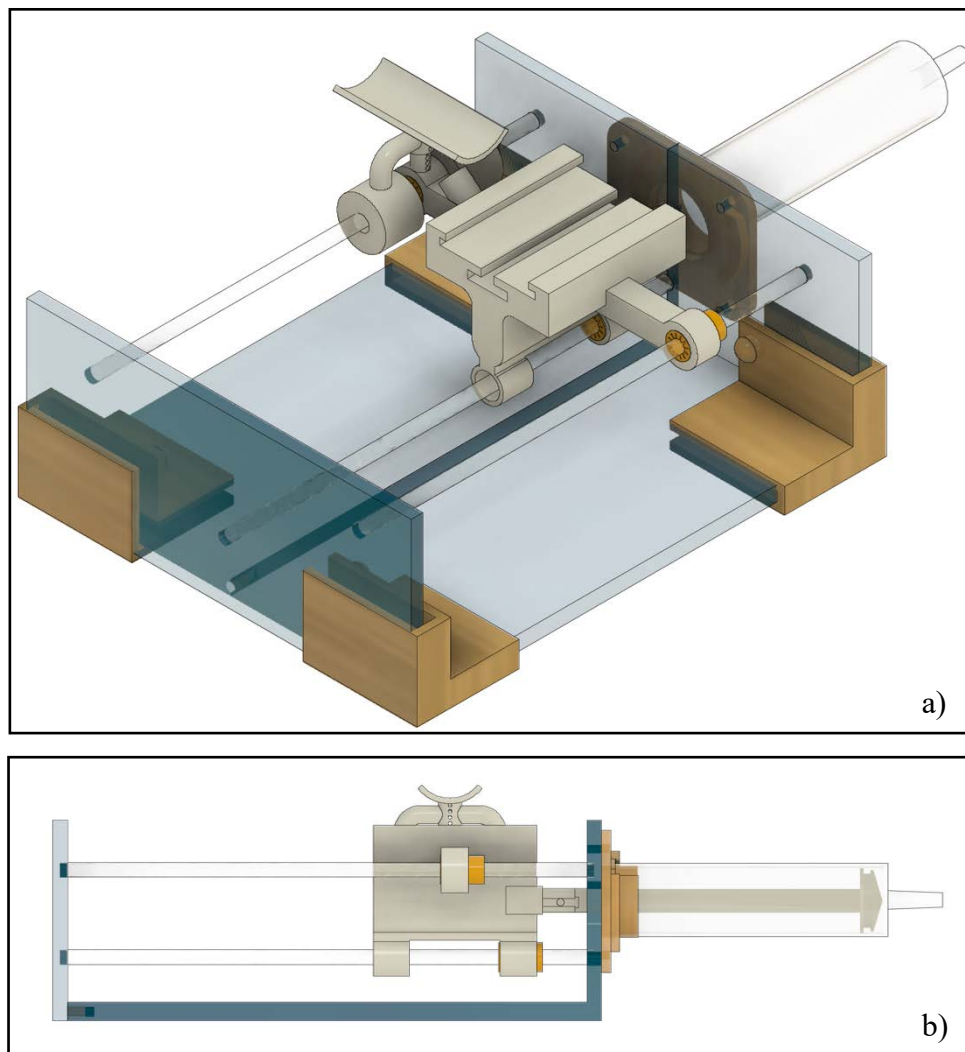


Figure 68: (a) Right front corner view of the alternate linear motion mechanism with the use of the support syringe slider. (b) Right side view of the linear motion mechanism with the use of the support syringe slider.

10.2.7 Assembly Piece

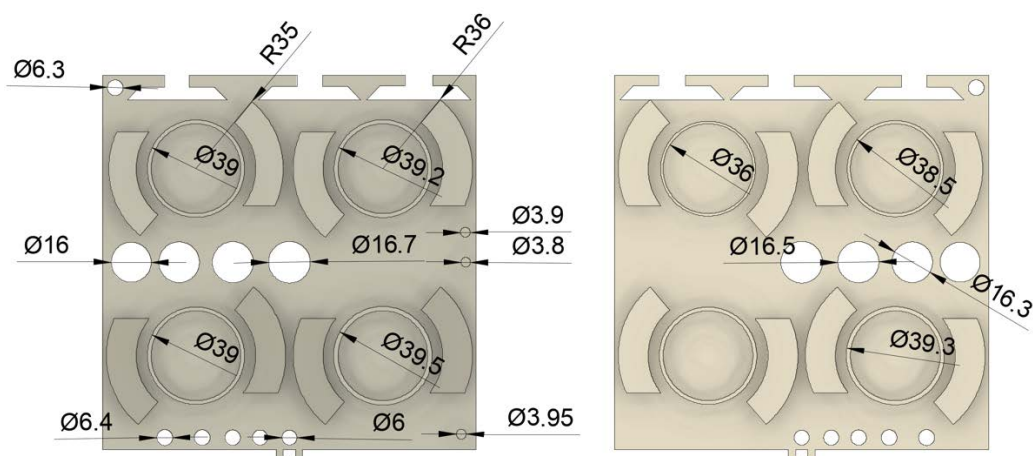


Figure 69: Detailed front (on the left) and back view of the assembly test piece.

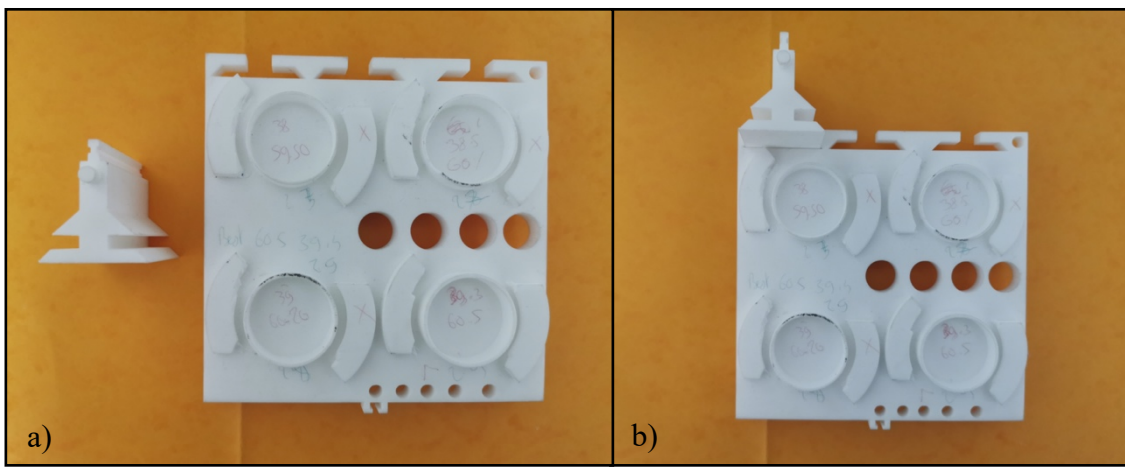


Figure 70 : a) Top picture of the assembly test piece and key piece. b) Top picture of the key pieces used to test the first version of the linear guided slot design (see 10.2.8).

10.2.8 Initial Linear Guided Slot & Frame Design

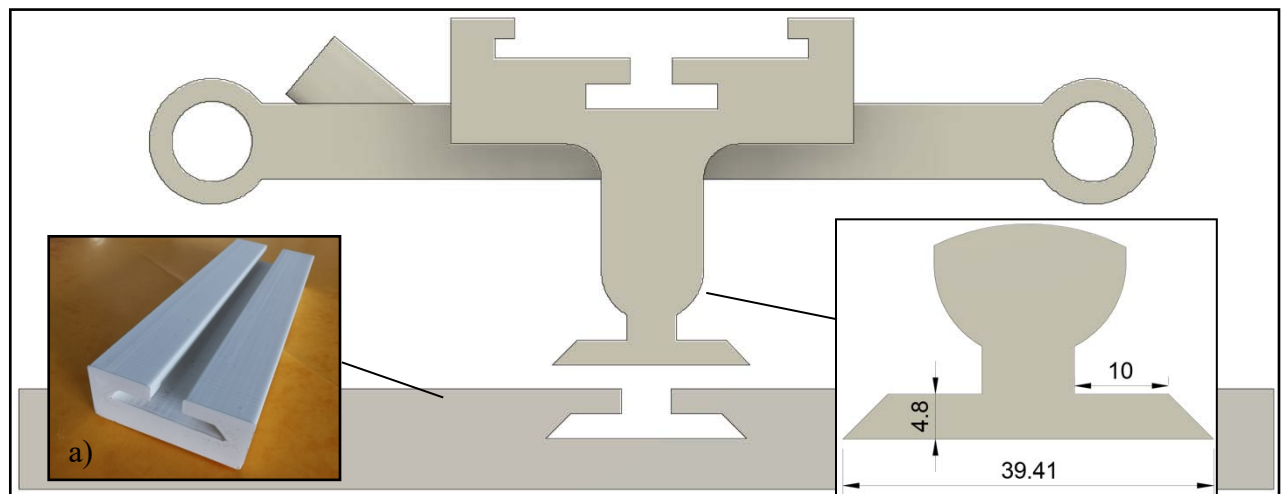


Figure 71: Front view of the initial version of the linear guided slot and frame (a).

10.2.9 Rib

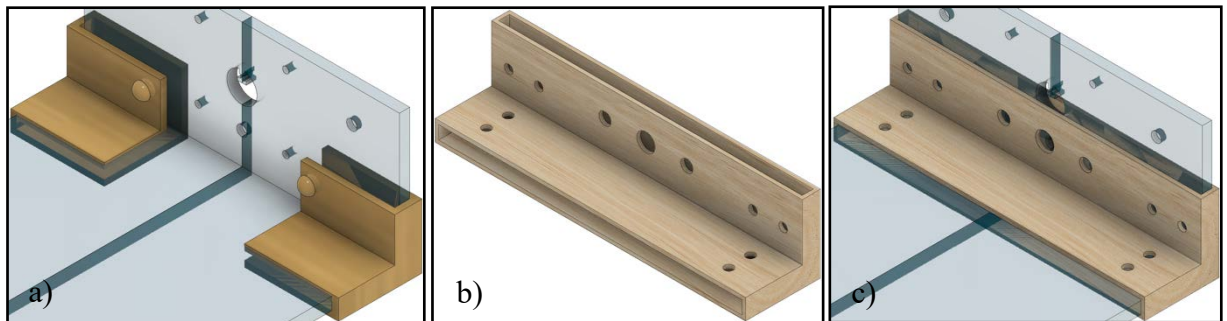


Figure 72: Different version of the rib like pieces to hold the acrylic frames together. The former version is shown in b), c) whereas the current version is shown in a).

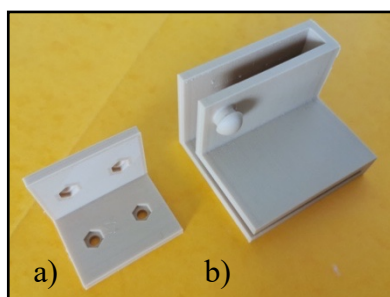


Figure 73: a) Initial version of the rib like pieces. b) current version of the rib like piece.

10.3 The Code

The code was adapted and modified from (22).

```
#define stepper_pin 9 // Pin 9 connected to Steps pin on EasyDriver
#define direction_pin 8 // Pin 8 connected to Direction pin
#define MS1 10 // Pin 10 connected to MS1 pin
#define MS2 11 // Pin 11 connected to MS2 pin
#define SLEEP 12 // Pin 12 connected to SLEEP pin

#define X_pin A0 // Pin A0 connected to joystick x axis
#define Joystick_button 4 // Pin 4 connected to joystick switch

#define Limit01 2 // Pin 2 connected to Limit switch out
#define Limit02 3 // Pin 3 connected to Limit switch out

int stepper_motor_speed = 10; // The higher the value of stepper_motor_speed, the slower the motor rotates.

void setup() {
    pinMode(MS1, OUTPUT);
    pinMode(MS2, OUTPUT);
    pinMode(direction_pin, OUTPUT);
    pinMode(stepper_pin, OUTPUT);
    pinMode(SLEEP, OUTPUT);

    pinMode(Limit01, INPUT);
    pinMode(Limit01, INPUT);

    pinMode(Joystick_button, INPUT_PULLUP);

    digitalWrite(SLEEP, HIGH); // Wake up EasyDriver
    delay(5); // Wait for EasyDriver wake up

    /* Configure type of Steps on EasyDriver:
     * MS1 MS2
     *
     * // LOW LOW = Full Step //
     * // HIGH LOW = Half Step //
     * // LOW HIGH = A quarter of Step //
     * // HIGH HIGH = An eighth of Step //
     */
}

digitalWrite(MS1, LOW); // Configures to Full Steps
digitalWrite(MS2, LOW); // Configures to Full Steps
}

void loop() {
    if (!digitalRead(Joystick_button)) { // If Joystick button is clicked
        delay(300); // delay for debouncing
    }
}
```

```

switch (stepper_motor_speed) { // check current value of stepper_motor_speed and change it
    case 1:
        stepper_motor_speed = 30; // slow speed
        break;
    case 3:
        stepper_motor_speed = 1; // fast speed
        break;
    case 10:
        stepper_motor_speed = 3; // medium speed
        break;
    }
}

if (analogRead(X_pin) > 712) { // If joystick is moved Left
    if (!digitalRead(Limit01)) {} // check if limit switch is activated

    else { // if the limit switch is not activated, then move the stepper motor clockwise

        digitalWrite(direction_pin, LOW); // (HIGH = anti-clockwise / LOW = clockwise)
        digitalWrite(stepper_pin, HIGH);
        delay(stepper_motor_speed);
        digitalWrite(stepper_pin, LOW);
        delay(stepper_motor_speed);
    }
}

if (analogRead(X_pin) < 312) { // If joystick is moved right

    if (!digitalRead(Limit02)) {} // check if limit switch is activated

    else { // if the limit switch is not activated, then move the stepper motor counter-clockwise

        digitalWrite(direction_pin, HIGH); // (HIGH = anti-clockwise / LOW = clockwise)
        digitalWrite(stepper_pin, HIGH);
        delay(stepper_motor_speed);
        digitalWrite(stepper_pin, LOW);
        delay(stepper_motor_speed);
    }
}

```

11.0 Shreya's Design

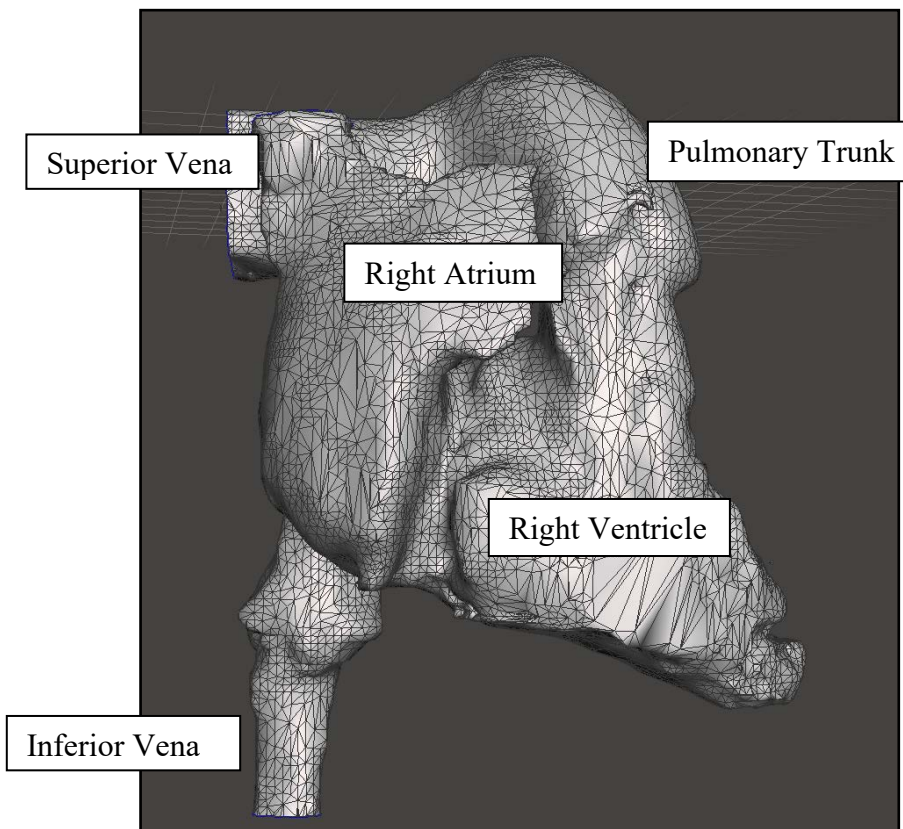


Figure 74: A front view of the 3D model created prior to mesh cleaning using Autodesk Meshmixer. Blood would usually flow from the SVC and IVC into the right atrium, right ventricle and out through the pulmonary trunk.

11.1 Methodology

In pulmonary arterial hypertension (PAH), there is a gradual rise in right ventricular afterload which leads to right ventricular hypertrophy in order to compensate for the increase in afterload, and alongside remodeling of the pulmonary arterial tree, this eventually causes an increase in pulmonary arterial pressure. The information used to create this 3D model was obtained from the MRI scans of a female pediatric patient, around 9 years old, with PAH. From those MRI images, she segmented out structures from the right side of the heart (the SVC and IVC, right atrium, right ventricle and pulmonary arteries)(Fig74). The software used to do this was Materialise Mimics, and the DICOM file containing the patient data was imported into the software before the segmentation process. After separating out the right heart from its surrounding tissues, the result was an STL file that contained a 3D ‘shell’ of the model which was then refined using Autodesk Meshmixer. This

process involved smoothing out the surface to aid printing of the model and creating connectors where necessary.

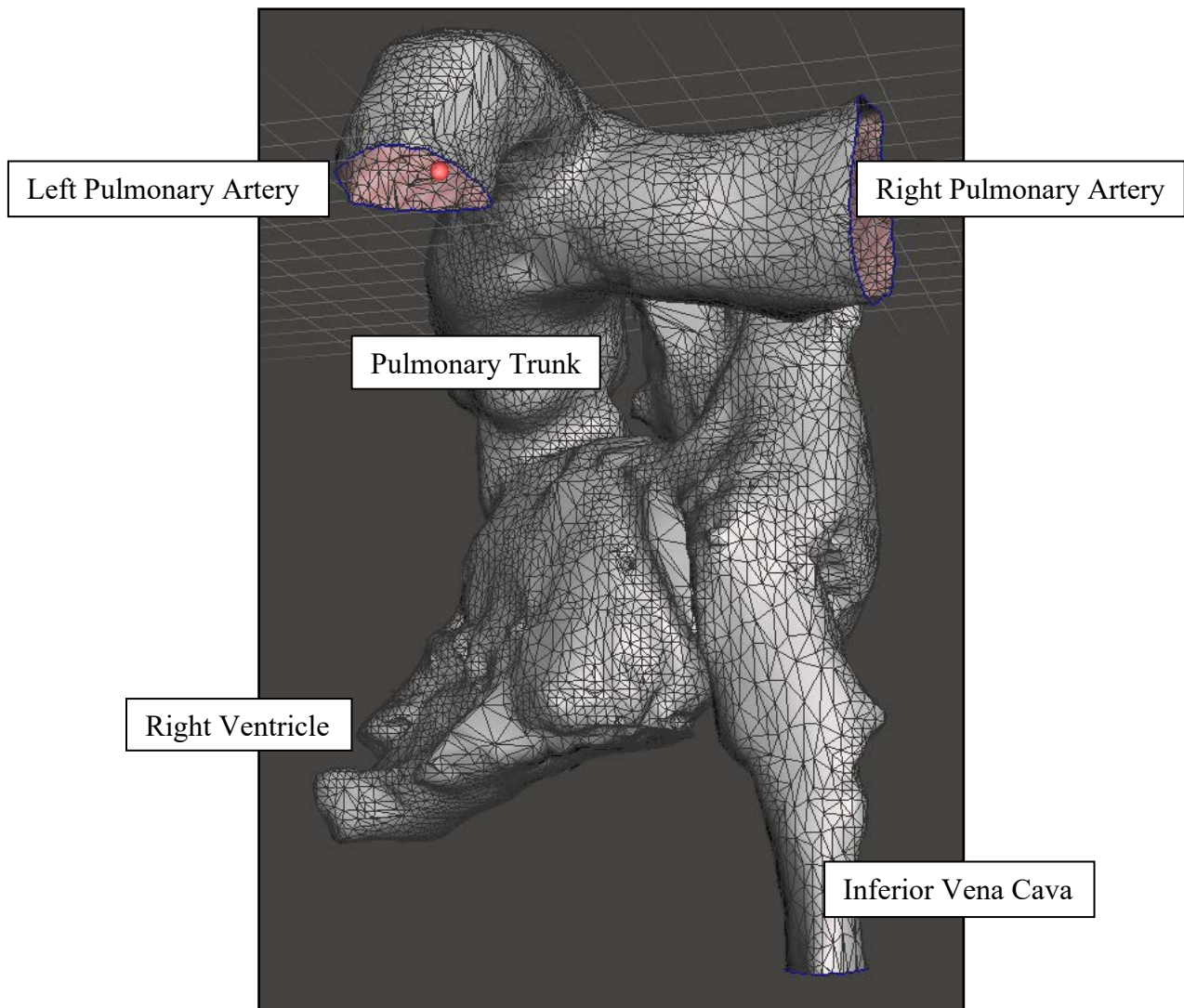


Figure 75: A posterior view of the 3D model created prior to mesh cleaning using Autodesk Meshmixer. The pulmonary trunk divides into the left and right pulmonary arteries.

11.2 Connector Piece

In this case, a connector (Fig 76) would need to be attached below the IVC as (Fig 74, 75), as the IVC would then be attached to a pump from the mock circulatory system during the experiments carried out for testing. The connector would then be attached to an inlet from a pump, such as the Harvard Apparatus Pulsatile Blood Pump, to simulate the flow of blood up through the IVC and into the right side of the heart. The secondary part of the connector shown in Fig 76 can be used to insert the catheter into the IVC as well, and any remaining space between the catheter and the tube would then be taped off to prevent fluid from leaking out of the mock circulatory system. It provides useful measurements including pulmonary pressures, cardiac output and pulmonary vascular resistance.

The entrance to the SVC was closed off using Autodesk Meshmixer, as well as the entrance to the right pulmonary artery; this ensures that there is only one inlet to attach to the mock circulatory system (the IVC) and one outlet (the left pulmonary artery). Fig77 show the final 3D model post-editing, where the IVC has an extra attachment below it that would allow the connector to be joined to the IVC after the parts are separately printed.

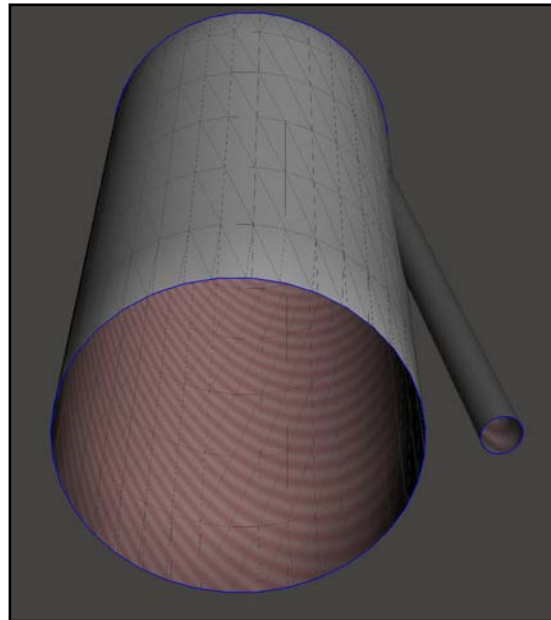


Figure 76: The inferior view of an example connector which could be attached to the IVC to set up the mock circulatory system. The first part of the connector is the large hollow tube with the correct diameter to allow attachment to the pump apparatus on one end and attachment to the IVC on the other end. The secondary part of the connector is the smallest hollow tube on the right, with the correct diameter to allow insertion of the catheter through this smaller tube without fluid leaking out of the mock circulatory system.

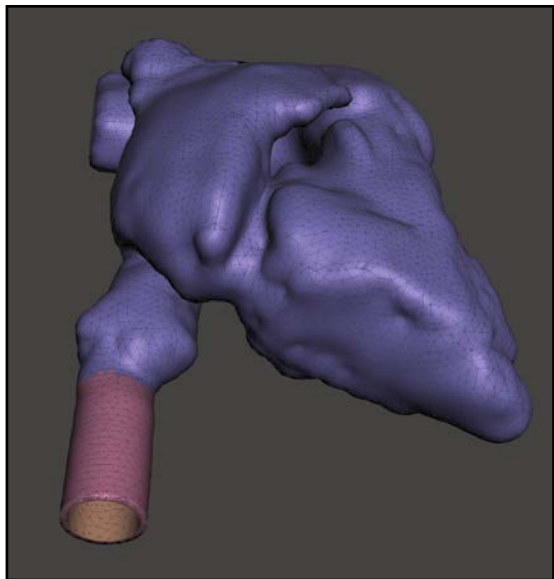


Figure 77: The refined 3D model, where the ventricular surface has been smoothed and the IVC remains open, with a cylindrical attachment below it where the extra connector piece would be attached.